Naval Research Laboratory
Washington, DC 20375-5320

NRL/MR/8140--00-8450

Notes On Improved Exponential Troposphere Model

JUNHO CHOI
SUNG KWAK

Command Control Communication Computers & Intelligence
Space Systems Development Department

April 17, 2000

REPORT DOCUMENTATION PAGE

Form Approved
OMB No. 0704-0188

1. AGENCY USE ONLY (*Leave Blank*)	2. REPORT DATE	3. REPORT TYPE AND DATES COVERED
	April 17, 2000	Final

4. TITLE AND SUBTITLE

Notes on Improved Exponential Troposphere Model

5. FUNDING NUMBERS

6. AUTHOR(S)

Junho Choi and Sung Kwak

7. PERFORMING ORGANIZATION NAME(S) AND ADDRESS(ES)

Naval Research Laboratory
Washington, DC 20375-5320

8. PERFORMING ORGANIZATION REPORT NUMBER

NRL/MR/8140--00-8450

9. SPONSORING/MONITORING AGENCY NAME(S) AND ADDRESS(ES)

SPAWAR, Code 9110
Washington, DC 20375-5320

10. SPONSORING/MONITORING AGENCY REPORT NUMBER

11. SUPPLEMENTARY NOTES

12a. DISTRIBUTION/AVAILABILITY STATEMENT

Approved for public release; distribution unlimited.

12b. DISTRIBUTION CODE

13. ABSTRACT (*Maximum 200 words*)

Atmospheric data extraction and processing procedures are presented for four different Databases: ECM, HIRAS, MRF, and FNL. Details of database utility are described for application of geolocation measure and semi-major/semi-minor axis EEP plot generation with miss-distance calculation procedure. New improved Exponential troposphere model algorithm has great utility reducing in processing time as well as improving geolocation accuracy by more than 50% for both performance and speed with storage requirements of databases.

14. SUBJECT TERMS

Troposphere	SMI	TOA
Miss-distance	TDOA	Geolocation
SMA	AOA	Exponential model

15. NUMBER OF PAGES

43

16. PRICE CODE

17. SECURITY CLASSIFICATION OF REPORT	18. SECURITY CLASSIFICATION OF THIS PAGE	19. SECURITY CLASSIFICATION OF ABSTRACT	20. LIMITATION OF ABSTRACT
UNCLASSIFIED	UNCLASSIFIED	UNCLASSIFIED	UL

NSN 7540-01-280-5500

Standard Form 298 (Rev. 2-89)
Prescribed by ANSI Std 239-18
298-102

CONTENTS

1. Introduction

Radio signals that pass through the Earth's atmosphere are sensitive to electrically neutral particles that cause a time delay in the signal depending on the dielectric constant of the media and path length. Additionally, if the signal does not travel in parallel with the density gradient of the atmosphere, it will be subject to atmospheric refraction, causing its path to deviate from a straight line. Geometrical bending of the signal path is greatly intensified in the lower atmosphere, most notably the troposphere, due to the curvature of the air layer near the Earth's surface. This bending effect on atmosphere is significant at low (ground station-to-spacecraft) elevation angles (less than 3 degrees). Consequently, an improved modeling technique (exponential tropospheric model or Choi model) for an excess propagation delay due to the atmosphere must be incorporated into the geolocation measurement software in order to take full advantage of propagation delay and to reduce the effect of elevation angle dependent errors induced by projecting the calibrated delays along the ground station-to-spacecraft line of sight.

The tropospheric propagation model currently implemented in the geolocation accuracy program is based on the elevation angle dependent model developed by Hopfield [1]. In the geolocation program, the weight function is used as the inverse covariance of noise Time Difference of Arrival (TDOA), ephemeris error, altitude error, and atmosphere error. This weight function is used to evaluate a miss distance and an ellipse uncertainty Semi-Major Axis and Semi-Minor Axis (SMA and SMI). The current geolocation system used the Hopfield atmosphere propagation delay model to compute the atmosphere error. At below 0 degree elevation angle from the horizon, the Hopfield model ignored (cut off) tropospheric propagation delay. This means that the atmospheric covariance among the weight functions is neglected in computing a miss distance and ellipse containment or that the measurements for TDOA below 0 degree from the horizon are considered as bad measurements. Also, the Hopfield model uses a constant refractivity for the entire world. In this report, the exponential tropospheric model, which provides the tropospheric propagation delay, even at negative elevation angles, is used to improve the geolocation accuracy program. The exponential tropospheric model is derived analytically by the mathematical formulation and required minimum inputs for the user. This exponential model generates the refractivity and bending error adaptively by reading real time surface meteorological data (temperature, pressure, dew point or relative humidity) in order to process more accurate results of tropospheric effects and was built as a library function to ease the interface with any other applicable system.

In this report the chronology of the tropospheric software and database development effort is presented. Section 2 presents the improved real-time tropospheric program and the binary database. Section 3 describes the data extraction and processing of the procedure for FNL data used to generate binary format databases for the tropospheric program. Section 4 shows the results of the application of the tropospheric program into the geolocation process. The geolocation accuracy of the Choi model improves approximately 50% as reflected in the SMA plots and miss distance calculations. In Section 5, conclusions and recommendations derived from this study are presented.

Manuscript approved March 16, 2000.

2. Improvement on Tropospheric Model and Database

The first version of tropospheric propagation model (Choi model) code [2] is designed as a subroutine package that can be incorporated into an application. All codes are written in the ANSI standard FORTRAN 77 with no machine dependent extensions except the VAX system. This program is divided into the Input/Output (I/O) data file processing and the main calculation. The I/O data files processing program reads two data files in ASCII format. The first contains weather data, including grid number, latitude, longitude, surface refractivity, pressure, temperature, and undulation of the geoid parameter. The second contains the reference height coefficient for each 2.5° x 2.5° grid. This part of the program invokes a database for the specified user location and sends it to the main part of the program to generate the tropospheric propagation effects. The main program calculates the time delay, range error, and angle of arrival error using the data files from the I/O part. The database contains the ACSII format data files for input data and output data files.

The new version of the tropospheric program has been converted from a FORTRAN version program to a C version program. This new C version program was upgraded with a new algorithm, and was built as a library function to easily interface with the other processors. The new version optimized the old version of the tropospheric program to adapt to the real time operational system, and converts the ASCII database format to binary format to reduce processing time and to save memory size. Figure 1 shows a functional block diagram for the new tropospheric propagation program. There are three major sections in the optimized tropospheric program: 1) input parameters and determination of the layer height and refractivity profiles; 2) the apparent angle computation to the given line of sight (LOS) elevation angle; and 3) the stratified method to calculate the time delay, range error, and angle-of-arrival error.

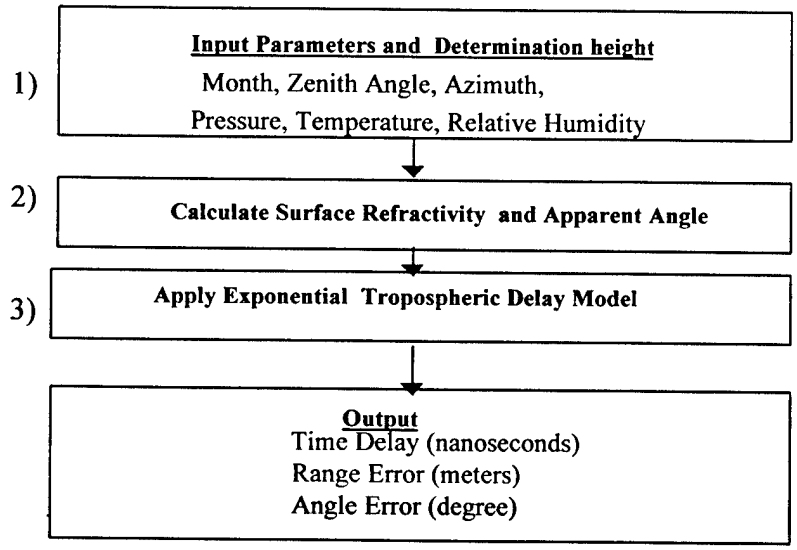

Figure 1. Functional Block Diagram of Exponential Tropospheric (Choi) Model

In this new version of the tropospheric model program, we assume that the ionospheric refractive effects are negligible above 400 MHz, that the refractive index gradient exists only in the vertical plane, and that the index of refraction profile can be approximated by a number of linear segments whose thickness is small compared to the earth's radius.

2.1 Tropospheric Propagation Model Program

In order to interface with any real time processor, the tropospheric delay program must be implemented as a library routine that can be easily maintained, modified, and ported to support different real time operational platforms. This upgraded C-version of the tropospheric delay program was developed to meet real time data processing requirements. This version uses a macro substitution and file inclusion as a pre-processor. The mathematical functions such as square root, cosine, sine, tangent, and arctangent for the degree are defined as macros. The variables which are used more than twice are declared as "#define" statements. The input database sources are also defined as text substitution to pass the library function. For any other required input information and functions interfaced with library functions, "tropodelay.h" is used with "#include" statements. In order to reduce function generality and program readability, we declare one integer array, and two static arrays as global values. All functions and subroutines in this program have access to these global variables. All functions in the library should be modularized. This means that a program should be broken into small modules with one main module that calls the others through the proper sequence. The "tropodelay" function initially connects to the binary database to access the user's desired data. This function continuously calculates an apparent angle to the line-of-sight elevation angle from the ground station to a target, the troposphere delay outputs the error of range, the angle of arrival, and the time delay.

2.1.1 Tropospheric Height and Refraction Profile

The index of refraction in the troposphere is a function of such meteorological variables as temperature, pressure, and water vapor. In order to estimate the refractive effects of the troposphere, the index of refraction (n) for each layer height must be determined.

The new C-version program assumes that the troposphere region is stratified into 46 different height and constant refractivity profiles for each layer. The height profiles are increased every 100 meters between 0 and 1,000 meters, every 500 meters between 1,000 and 10,000 meters, and every 1,000 meters between 10,000 and the top of the troposphere region (27 km from the Earth's surface). The main reason for this division is based on the fact that the refractive effects are small above 10 km from the surface of the Earth. The test has been performed in order to validate this argument of 46 layers by

computing range and angle errors on different environments with spatial, temporal, and geographical variations in the previous study for more than 100 sites [2].

The refractive profiles are accomplished by a combination of the meteorological data supplied by the National Oceanographic and Atmospheric Administration (NOAA) and the National Weather Service (NWS) and the exponential tropospheric propagation model. The exponential tropospheric propagation model (Choi model) that the NRL has developed is used to estimate the refractivity ($N = 10^6[n-1]$) of the troposphere region (up to 27 Km from the Sea level) based on the height of 46 different profiles. The exponential tropospheric propagation profile is chosen because the refractivity of the observation and prediction is very close to real weather information of each layer in the troposphere region. The exponential model is theoretically based on the surface temperature, pressure, and relative humidity. Each component profile starts with a locally observed surface meteorological value and decreases to the effective troposphere height (27 Km). With this assumption, each layer refractivity is calculated by the exponential tropospheric model program. Empirical weather data is used in the calculation of refractivity for each of the layer profiles when local weather information is not available.

Figures 2 and 3 show the different time delays for different azimuth angles for February and August between the original ECM 14 layer data and the model defined by 46 layer, respectively, for 0 degree elevation angle from the ground to a target for 8 different locations (refer to Appendix). In these figures, the different time delays for azimuth angle ($0 \sim 360$ degree) are within $\pm$ 0.05 nanosecond for 8 different sites. Figures 4 and 5 present time delay differences between original ECM 14 layer data and model defined by 29 layer. Figures 6 and 7 show the time delay difference between ECM 14 layer data and the model defined by 14 layer. From these figures, the conclusion has been made to use 46 different layer profiles and heights because of their accuracy and closeness to the analytical result.

2.1.2 Apparent Angle Computation

Since the refractive index is not the same everywhere, the trajectory tends to be curved consequently. There is a difference between the real direction of the source and the apparent direction from which the propagation waves arrive. We have already seen, in the case of the troposphere, that in a spherically symmetrical medium the radius of curvature of the trajectory is proportional to the vertical gradient of the refractive index. The first version of the tropospheric program was used as an iterative approach to compute an apparent angle given the LOS (line-of-sight) elevation angle from the ground to satellite. Figure 8 presents the apparent angle computation algorithm using an iterative approach. If the angle error difference between a LOS angle and an estimated apparent angle is within a given threshold, the convergence is reached and the true incoming elevation angle is now known. An initial estimate of the elevation angle for the actual signal is obtained by adding a different angle of arrival error (AOA) to the LOS elevation angle

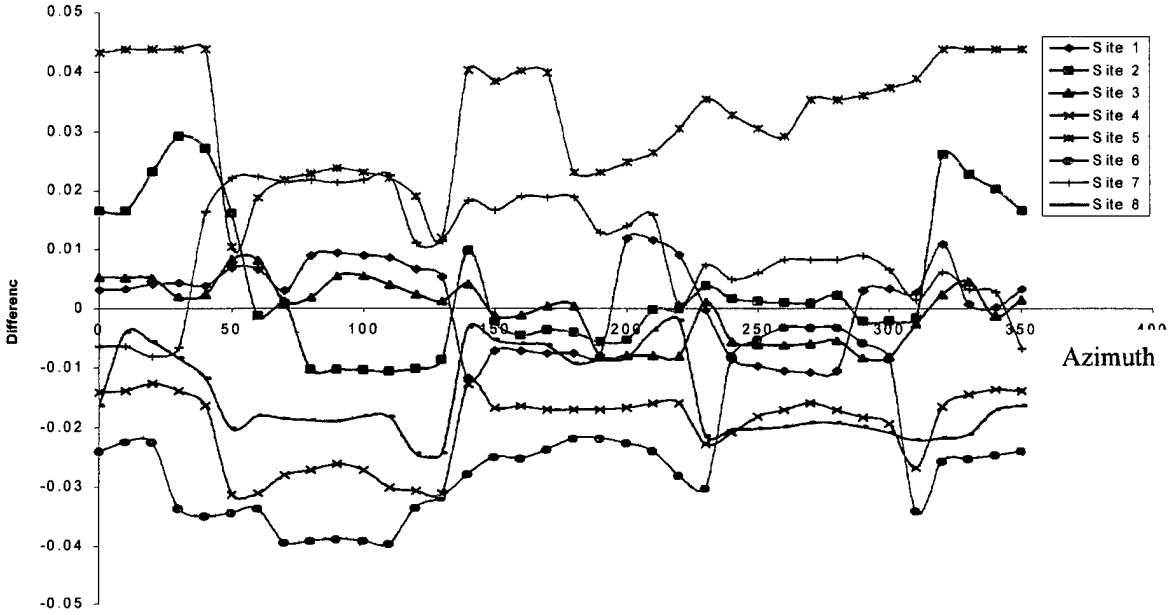

Figure 2. Difference of Time Delay (ECM 14 layer and model 46 layer) for February

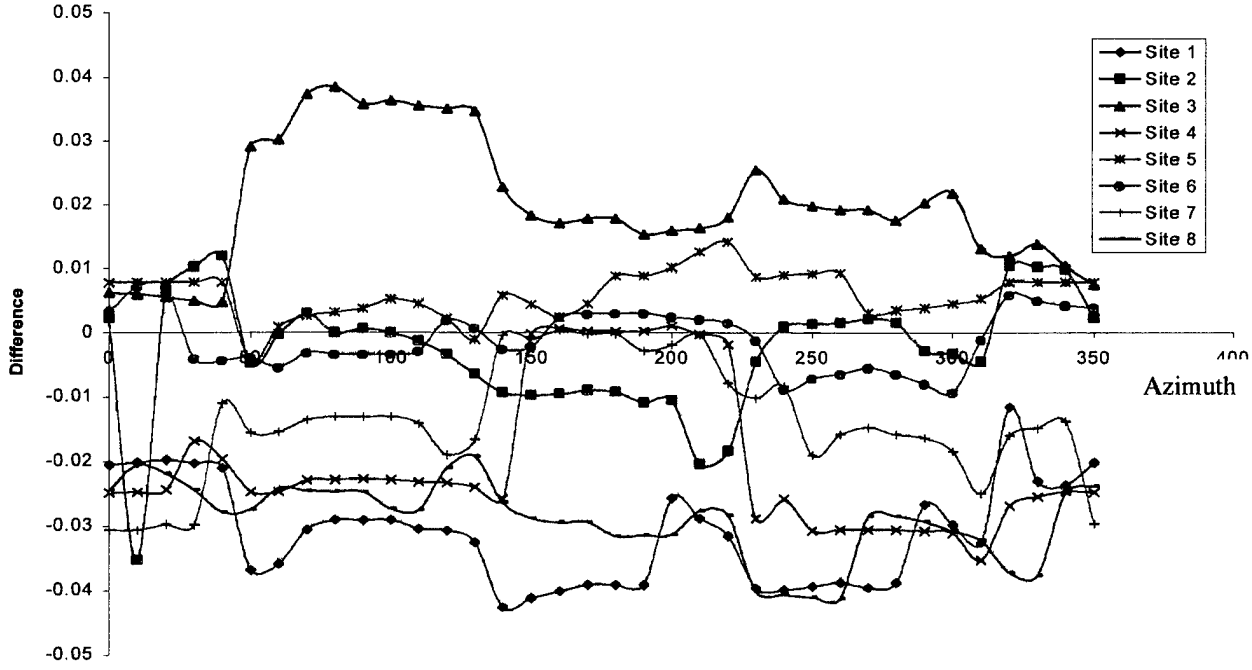

Figure 3. Difference of Time Delay (ECM 14 layer and model 46 layer) for August

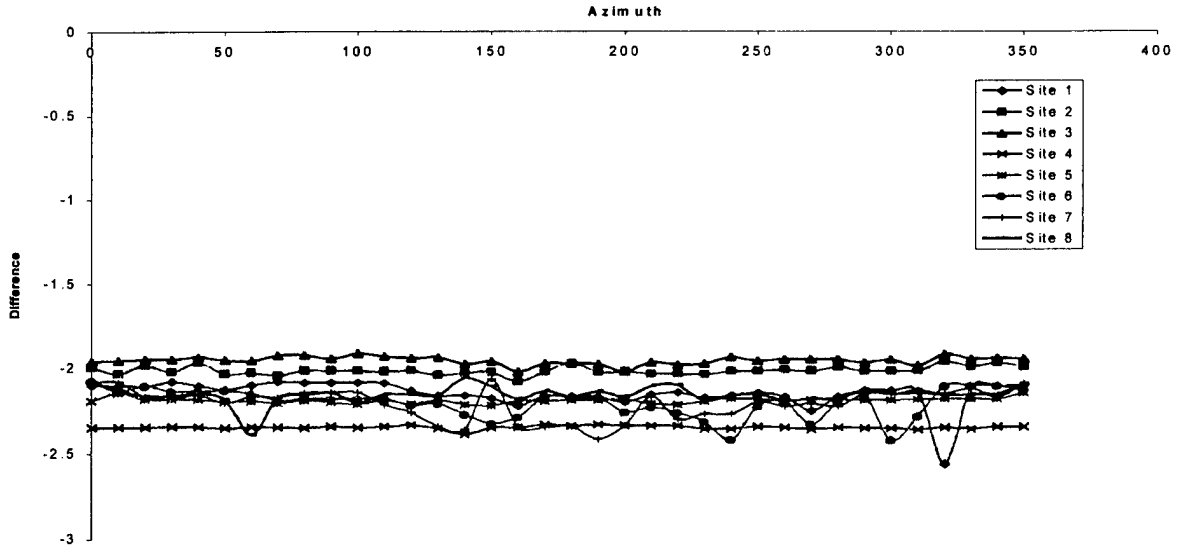

Figure 4. Difference of Time Delay (ECM 14 layer and model 29 layer) for February

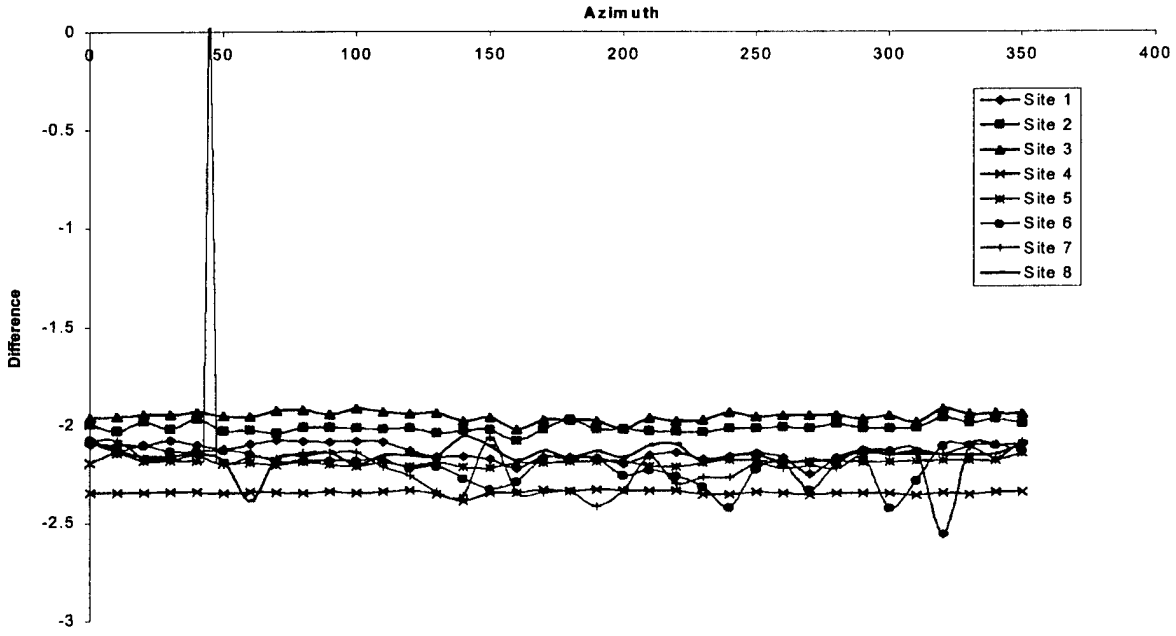

Figure 5. Difference Time Delay (ECM 14 layer and model 29 layer) for August

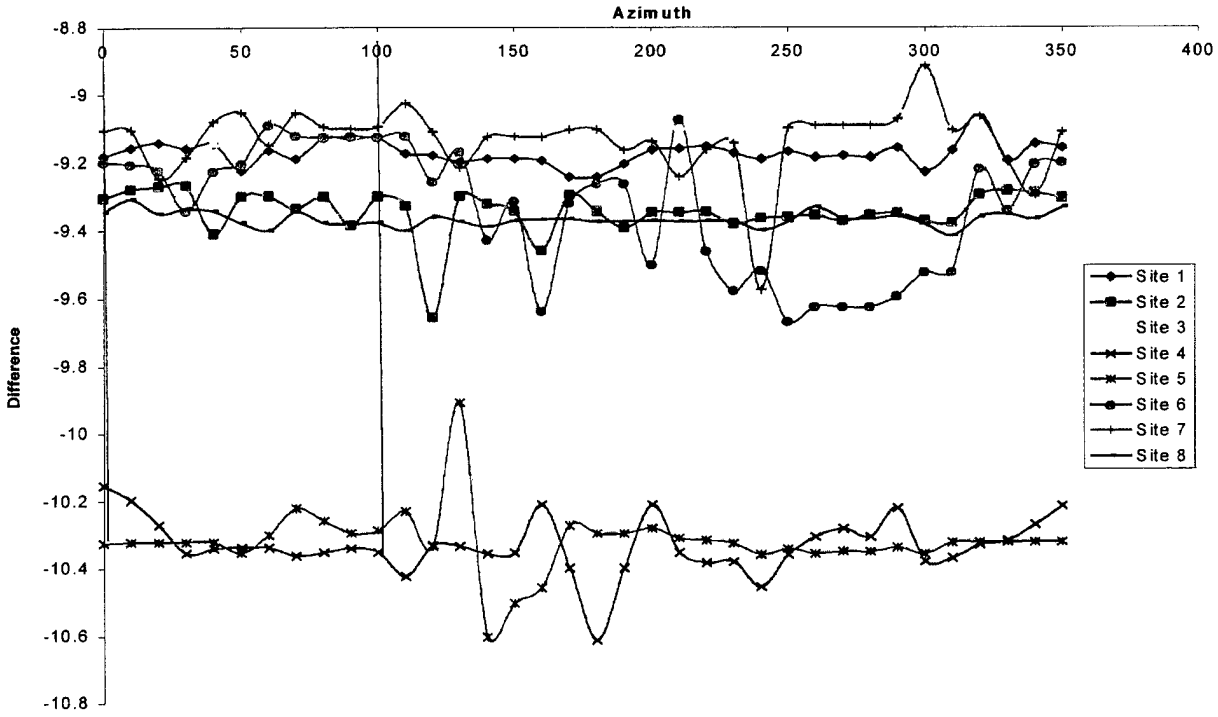

Figure 6. Difference of Time Delay (ECM 14 layer and model 14 layer) for February

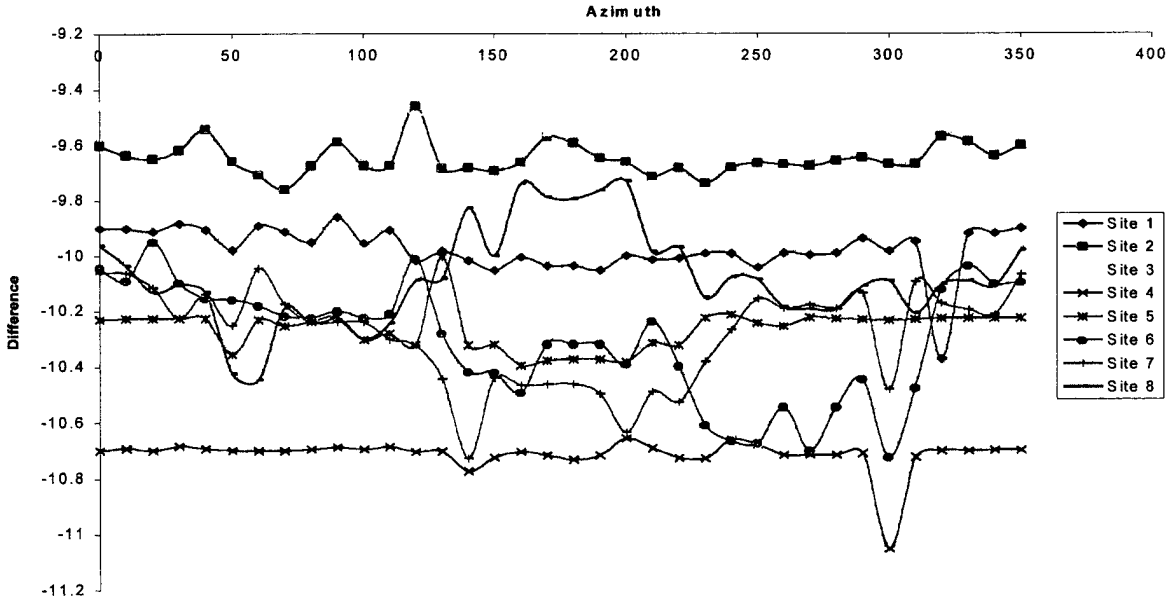

Figure 7. Difference of Time Delay (ECM 14 layer and model 14 layer) for August

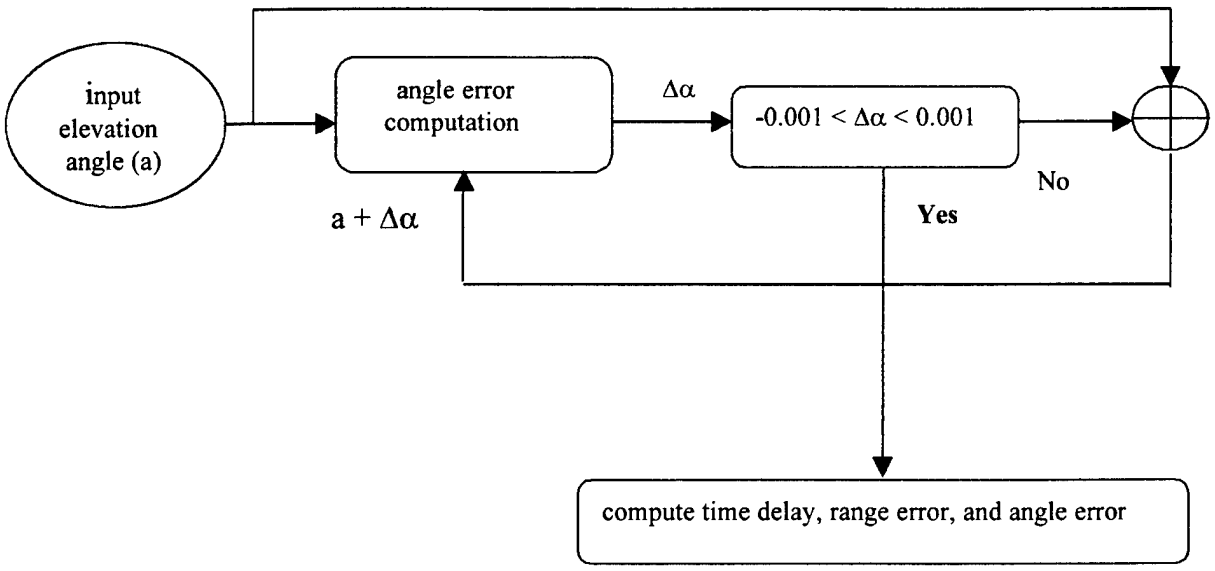

Figure 8. Iteration Method for Apparent Angle

Snell's law for spherical geometry and the stratified layer method with the refractivity height profile are used to compute the signal path at each location in the troposphere. If the deviation estimated apparent angle from the true LOS elevation angle is above a certain threshold, the process is repeated until convergence is reached. Above 10 degrees LOS elevation angle, the iteration loop is not necessary to reach the convergence condition. Below the 10 degree LOS elevation angle, more than one iteration loop is needed to satisfy the convergence condition. Below a 10 degree LOS elevation angle, at least 2 iteration loops are specifically requested. An iterative approach to compute the apparent angle for the refractive effect is not adaptable to the real-time processor because the processing time of the system is too long.

In order to reduce processing time of the real time processor, we have analyzed and developed a new algorithm for the apparent angle using the given input parameters of the troposphere propagation delay model. Figure 9 shows the angle error versus refractivity for all seasons to different LOS elevation angles. In this figure, the apparent angle can be predicted with the LOS elevation angle and surface refractivity, which is observed from simple surface measurements of the common meteorological elements of temperature, pressure, and relative humidity. Each linear equation is associated with the LOS elevation angle and the surface refractivity. The new statistical apparent angle computation is based on the slope and the intercept component of each linear equation. The apparent polynomial equation, which is combined with the slope and intercept component, is a function of the surface refractivity and the LOS elevation angle. This new algorithm was inserted in the new improved tropospheric propagation model program. Figure 10 is shown for the difference of time delay between the iterative approach and the statistical approach for the verification of the new algorithm for apparent angle computation of 8 different locations. In these figures, the absolute value of angle differences are within 0.3 nanosecond.

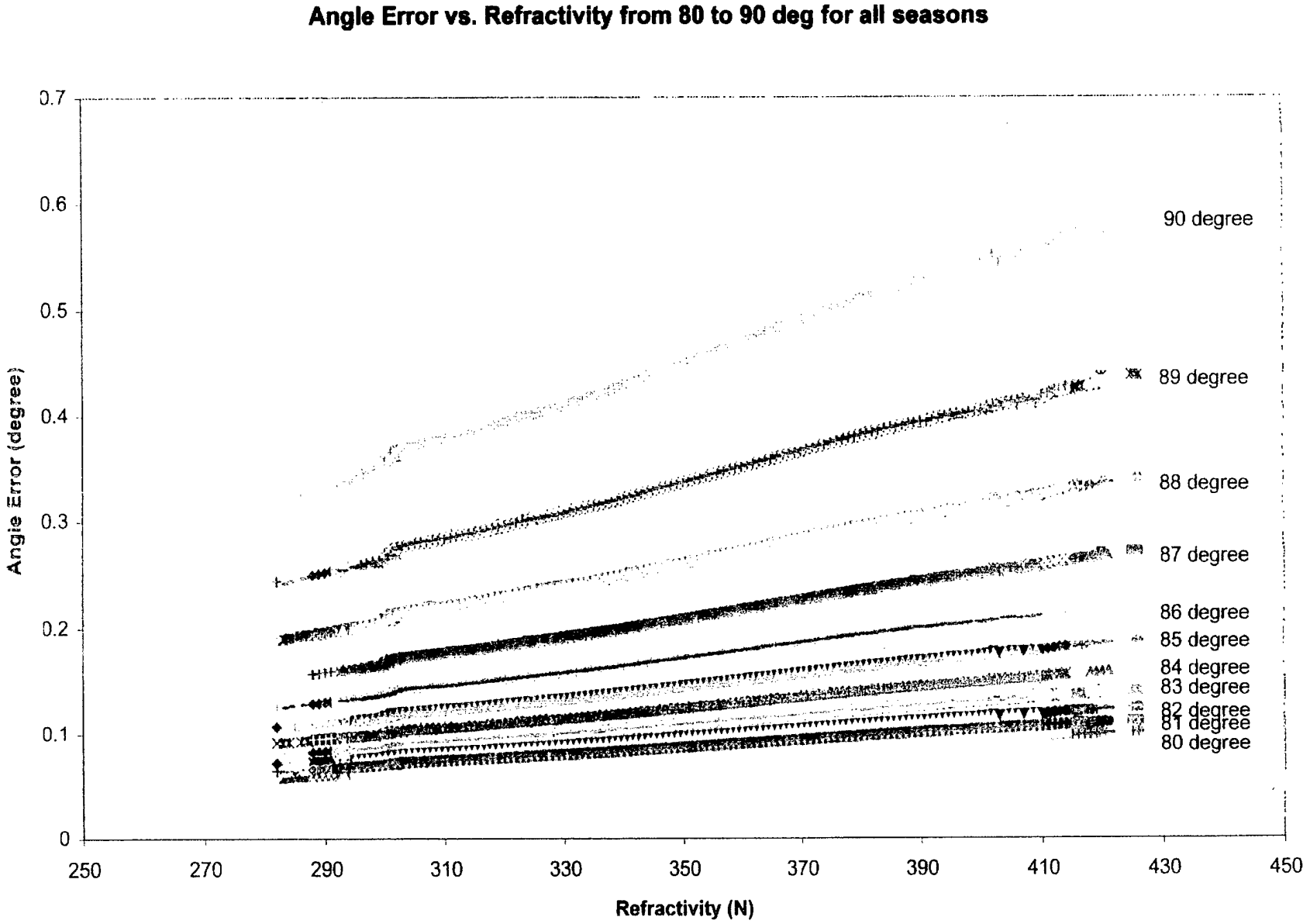

Figure 9. Angle Error vs. Refractivity for All Seasons

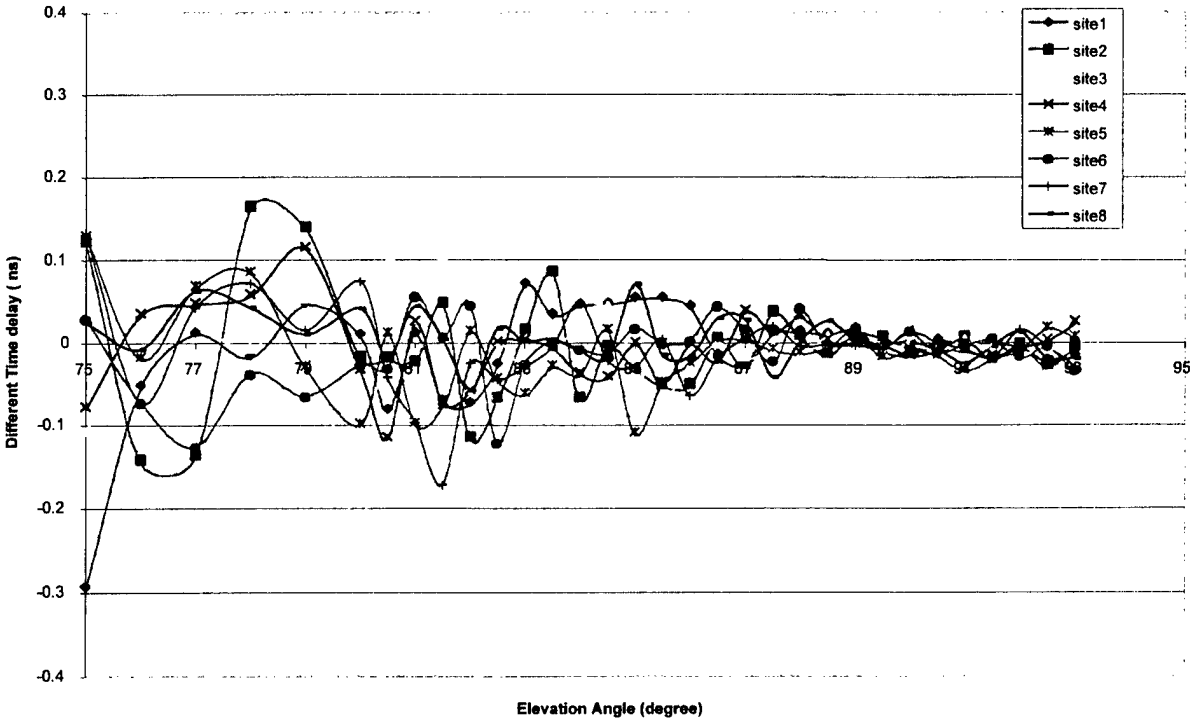

Figure 10. Time Delay Difference between Iteration and Statistical Approach

2.2 Procedure to Reduce Database and Extract Binary Data

The previous C-version of the tropospheric delay program only supported ASCII data files, which read sequentially within the inner loop when data is requested from a file. This process adds an additional overhead to the program execution time. This ASCII format database needs a huge storage space for high-resolution global data such as the MRF hourly and diurnal database. We found that the binary data format could be processed faster than ASCII format data. When we switched raw data to the binary format, we used a simple compression technique that converted floating point values (4 bytes) to integer values (2 bytes). The previous data access routine was invoked by the data based on the grid number from the database. In this new version, we used the record number instead of the grid number for direct access to the data and binary tree linked list approach. When the user selects input data information, the new program calculates the offset value for the record instead of going back to the grid number routine. Therefore, the new binary data format does not need to keep the grid number. This process saves 42 Kbytes for the ECM database, 168 Kbytes for HIRAS, and 61 Mbytes for MRF. Table 1 shows a comparison of the database size between ASCII and the binary format. The size of the database is reduced by up to approximately 50% for each database through the new program. The modified version will read binary files, and directly access to the data. The inner loop was then removed from file readings.

Table 1. Comparison of ASCII and Binary Format Size

	ASCII Format	**Binary Format**
ECM	2 Mbytes	1Mbytes
HIRAS	5.4 Mbytes	2.5 Mbytes
MRF (7 Years)	1.3 Gigabytes	636 Mbytes
FNL (Monthly)	384 Mbytes	109 Mbytes
FNL (Yearly)	4.7 Gigabytes	1.15 Gigabytes

ECM Binary Format – 'Yearly data' contains 10,368 records with 72 bytes for each record as shown in Figure 11. The first 24 bytes of the record contain surface refractivity data for 12 months. The last 48 bytes of the record contain the reference height data for the 12 months. Each monthly surface refractivity data must be read as 2 bytes unsigned integer or short. The first 2 bytes of the 24 bytes refer to the first month, the next 2 bytes of the 24 bytes refer to the second month, and so forth. To retrieve the actual refractivity value, you must extract the first 2 bytes of data related to the offset value, and then convert the two-byte integer value to an actual refractivity floating point divided by 100.0. Each monthly reference height data must be read as 4 bytes long. The first 4 bytes of the 48 bytes refer to the first month, the next 4 bytes of the 48 bytes refer to the second month, and so forth. To retrieve the actual reference height value, you must convert the extracted value to a floating point value and divide it by 100.0.

HIRAS Binary Format – 'Monthly 6 hourly data'. The HIRAS binary file is divided into monthly 6-hour blocks of data. Each monthly block of data consists of 124,416 bytes, and contains a 6-hour block of data for all 10,368 2.5° x 2.5° grids. Each grid block of data is 12 bytes in size as shown in Figure 12. The first 8 bytes contain 6-hour surface refractivity data, and the last 4 bytes contain the reference height data. The 0000-hour would be the first 2 bytes, the 0600 hour would be the next 2 bytes, and so forth. Surface refractivity data is read as 2 bytes unsigned integer or short. The extracting method of the actual value is the same as in the case of the ECM database.

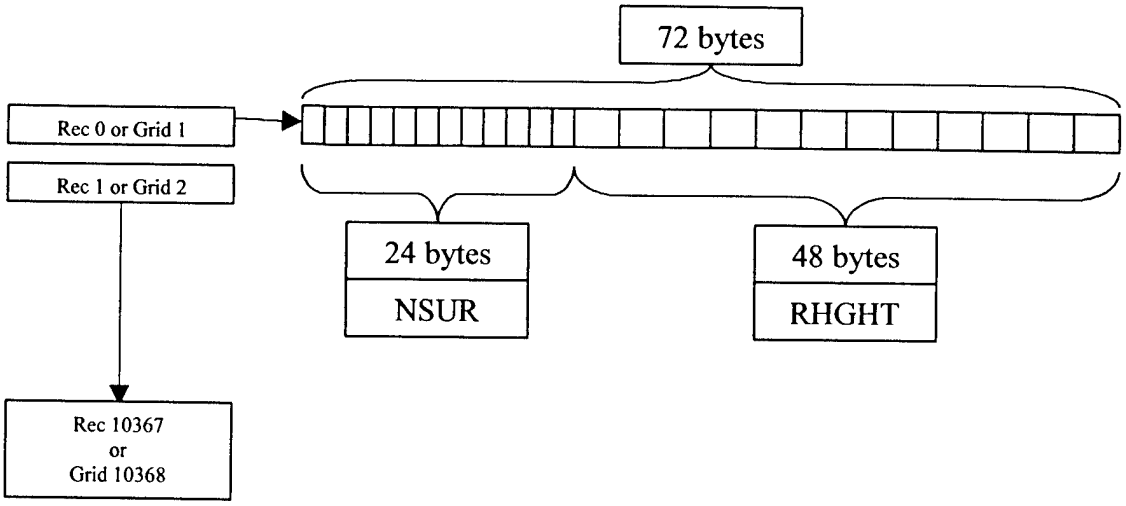

Figure 11. ECM Binary Format Structure

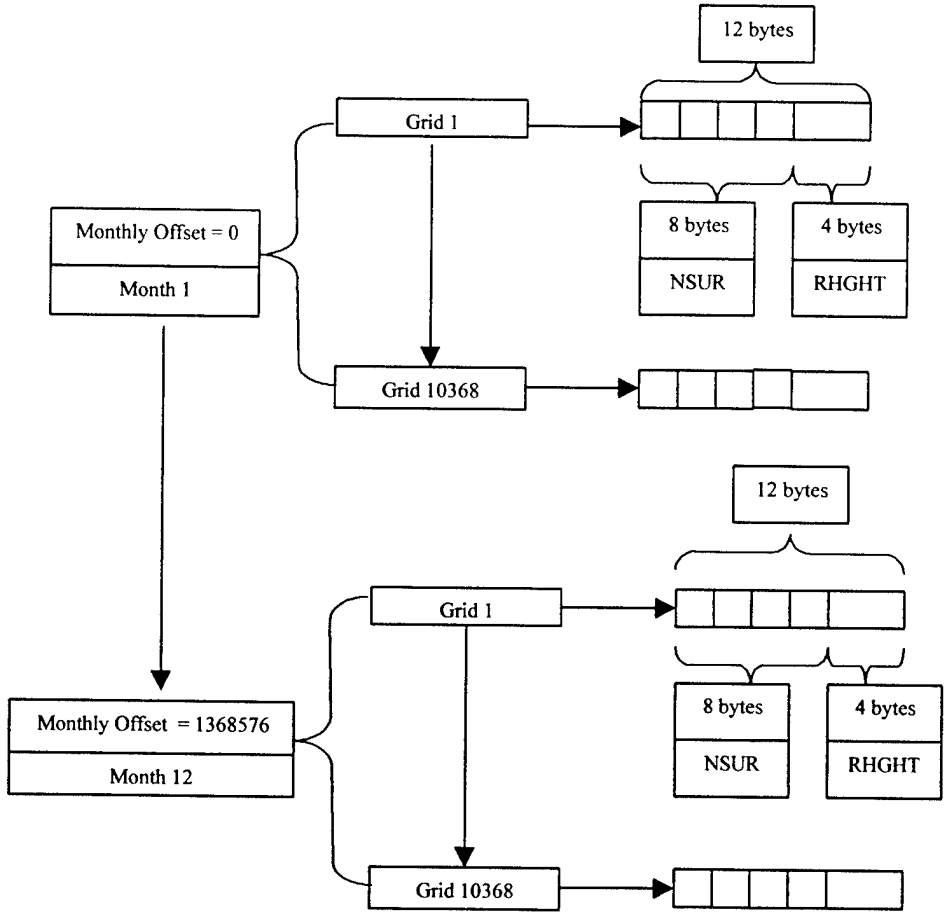

Figure 12. HIRAS Binary Format Sructure

MRF Binary Format – 'Daily 6-hour data'. The MRF binary file is divided into yearly binary files. Each yearly file contains 12 months of 6-hour daily data. Each 6-hour daily block of data is 248,832 bytes in size, and contains all 10,368 2.5° x 2.5° grids for that particular day. Each grid block of data is 24 bytes in size as shown in Figure 13. The first 8 bytes contain 6-hour surface refractivity data, and the last 16 bytes contain the 6-hour reference height data. The 0000-hour would be the first 2 bytes, the 0600 hour would be the next 2 bytes, and so forth. Surface refractivity data is read as 2 bytes unsigned integer or short. The last 16 bytes contain the 6-hour as it is reference height data. The 0000 hour would be the first 4 bytes out of the 16 bytes, the 0600 hour would be the next 4 bytes out of the 16 bytes, and so forth. Reference height data must be read as 4 bytes long. The actual value is extracted in the same method as for the case of ECM.

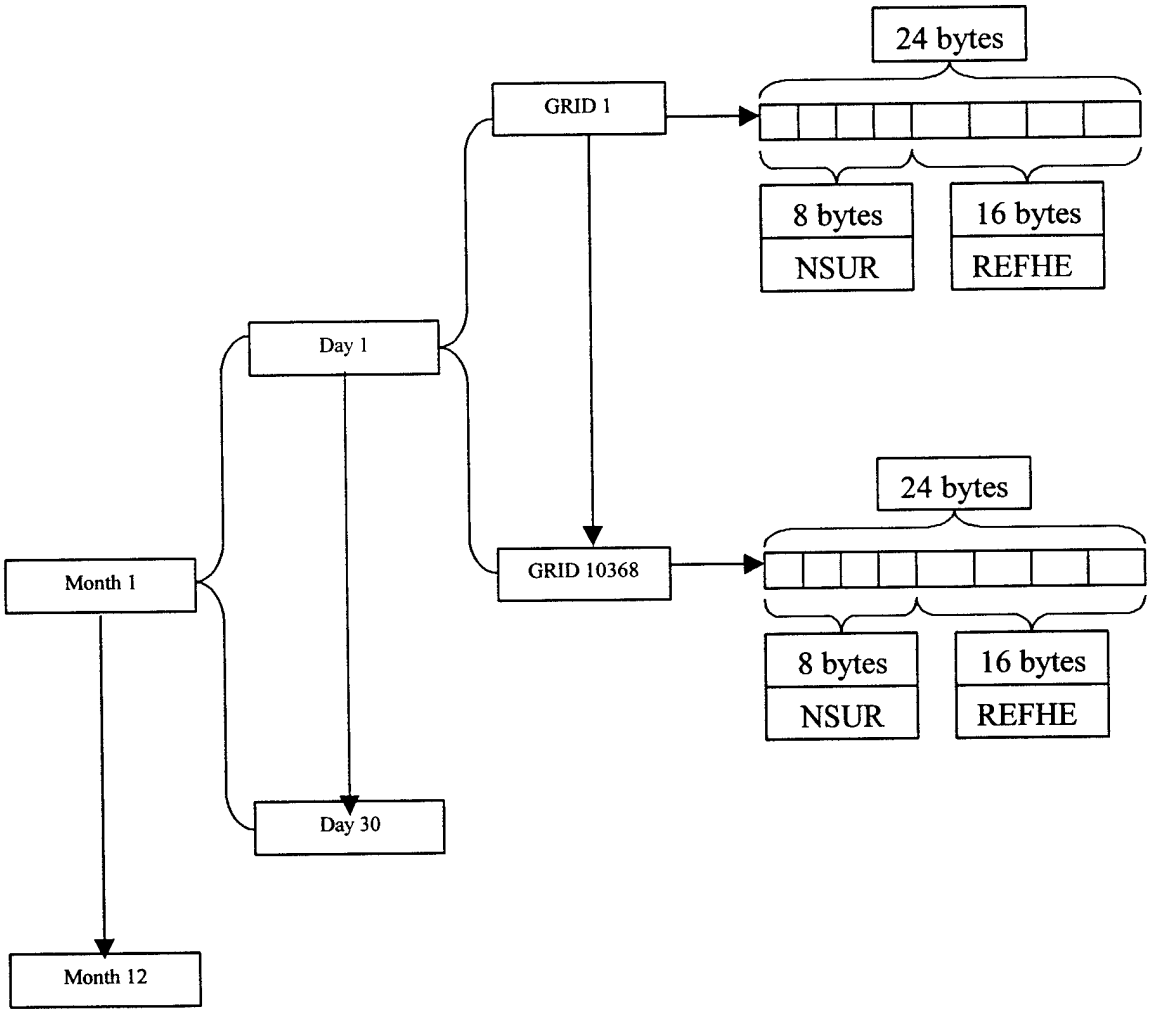

Figure 13. MRF Binary Format Structure

2.3 Performance Analysis and Simulation Results

The improved tropospheric exponential model with binary database has been examined to show the advantages and improvements of the new approach. Figures 14, 15, and 16 show global time delay errors for 1 degree, 0 degree, and –1 degree elevation angle from the horizon during August based on a 10-year average of climatology data from the ECMWF. Time delays vary from 180 nanoseconds in the shorter range to 620 nanoseconds in the longer range. This error reflects a 180 ft range error for the ideal cases without consideration of other atmospheric effects. Figures 17, 18, and 19 show contour plots of global time delay errors for the same elevation angle with the FNL data during August 15, 1997 at 00:00 Zulu time based on diurnal meteorological data from NOAA. Those figures show the different time delays between average database and real time database for the entire world. Table 2 shows the time delay comparison between a 10-year average empirical database (ECM) and real time data for 11 different locations from Figures 14 through 19. This table provides the time delay difference from the negative 3-degree elevation angle to the 10-degree elevation angle. The variation of time delay is noticeable. For below 3-degree elevation angle from the horizon, the time delay difference dramatically increases in the order of magnitude. The result of Table 2 indicates that the choice of the real-time data dominates the performance of the atmospheric propagation delay. This table shows that the time delays above a 5-degree elevation angle are not much different from those below a 3-degree elevation angle. Table 3 shows the angle of arrival error comparison from 10 degrees to negative 3 degrees between the exponential model and the Hopfield model using the real time FNL data August 1, 1999 data for 8 different locations. In this table, we know that the exponential model compensated more than 50% for any elevation angle. This wide error causes significant problems in satellite communication link analysis and antenna operator. The time delay and angle-of-arrival error produce a geolocation error of tens of nautical miles. If these errors are calibrated or corrected on time for the specific mission, valuable time and cost can be saved, and the accuracy will be dramatically increased.

The improved tropospheric exponential model with binary database reduces the processing time when we calculated time delay, range error, and angle of arrival error. Table 4 shows the average processing time for different layers with and without grid crossing. The processing times were computed by executing an iteration loop 3,600 times. The number in parenthesis represents the processing time of one iteration of the tropospheric program. The processing time of binary format is faster than ASCII format in this table.

3. Data Extraction and Processing Procedure

From March 1999 to date, we have processed the FNL and MRF database (1997 – present). We are currently developing an automatic and user friendly data processing software tool to produce the database for the new tropospheric program. The FNL data

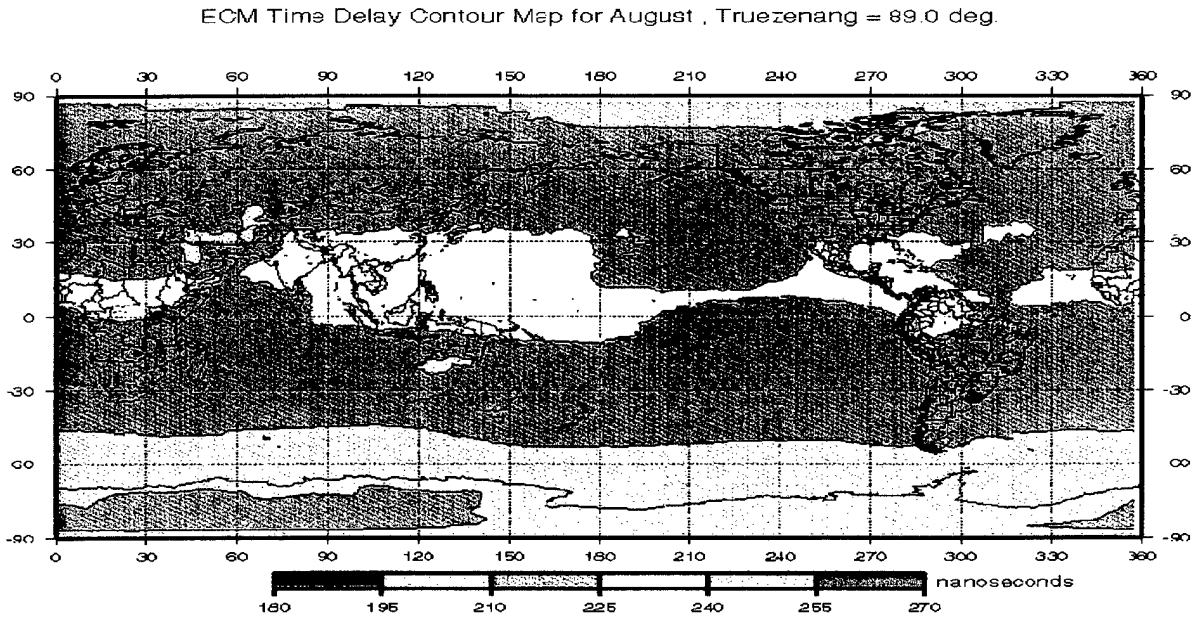

Figure 14. ECM Time Delay Contour Map for August (elevation angle = 1.0 deg)

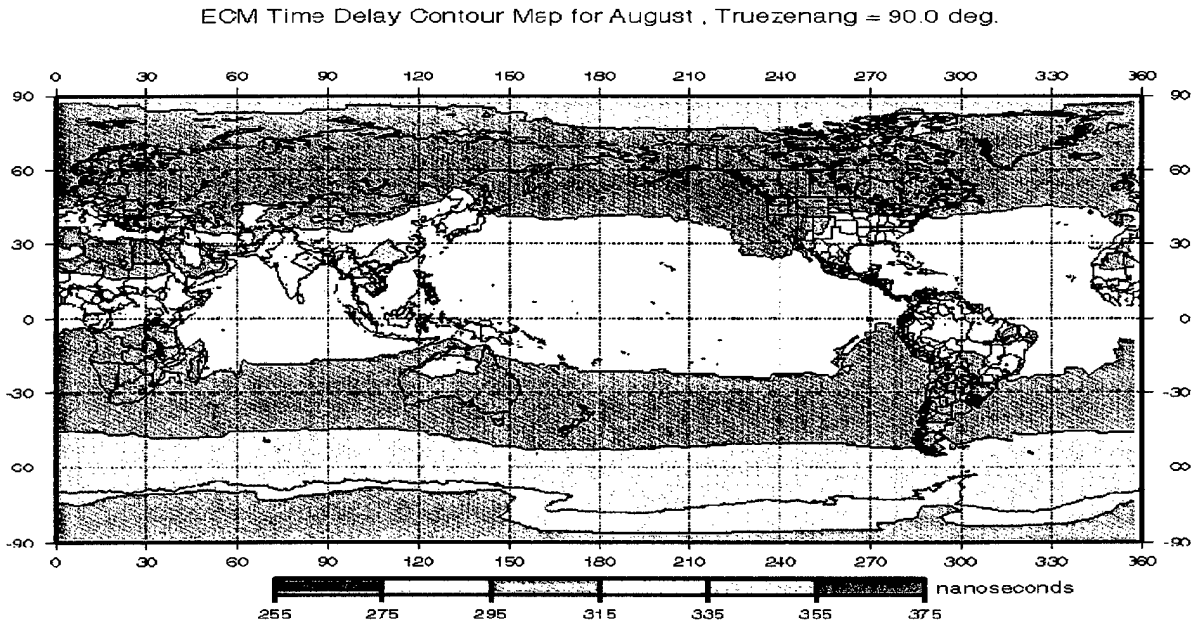

Figure 15. ECM Time Delay Contour Map for August (elevation angle = 0.0 deg)

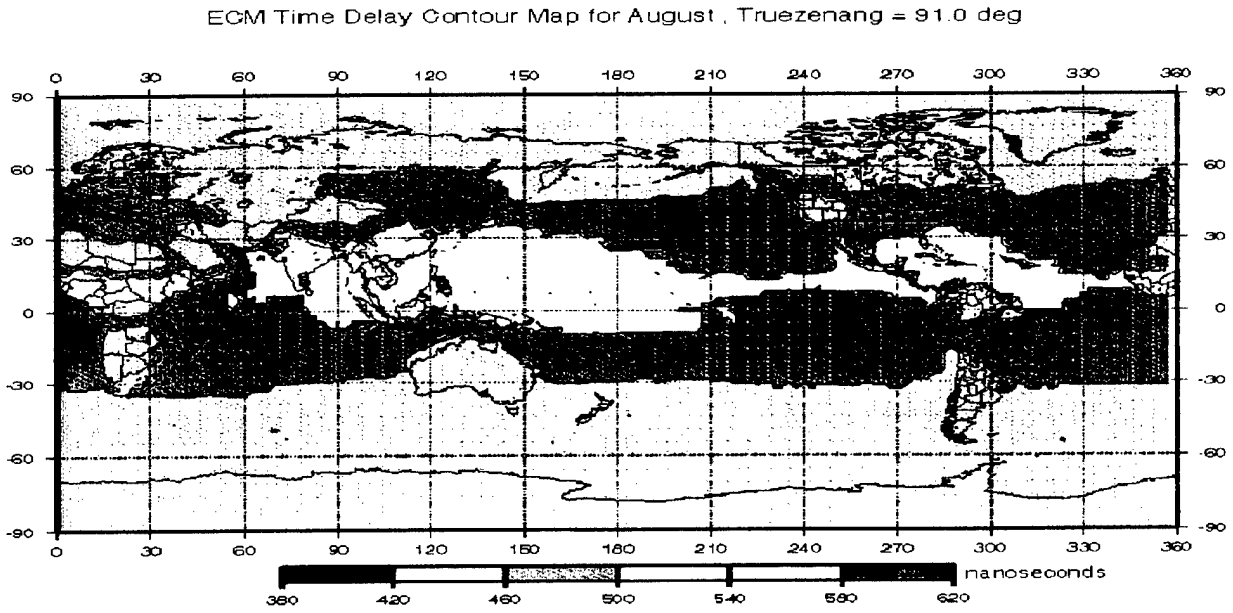

Figure 16. ECM Time Delay Contour Map for August (elevation angle = -1.0 deg)

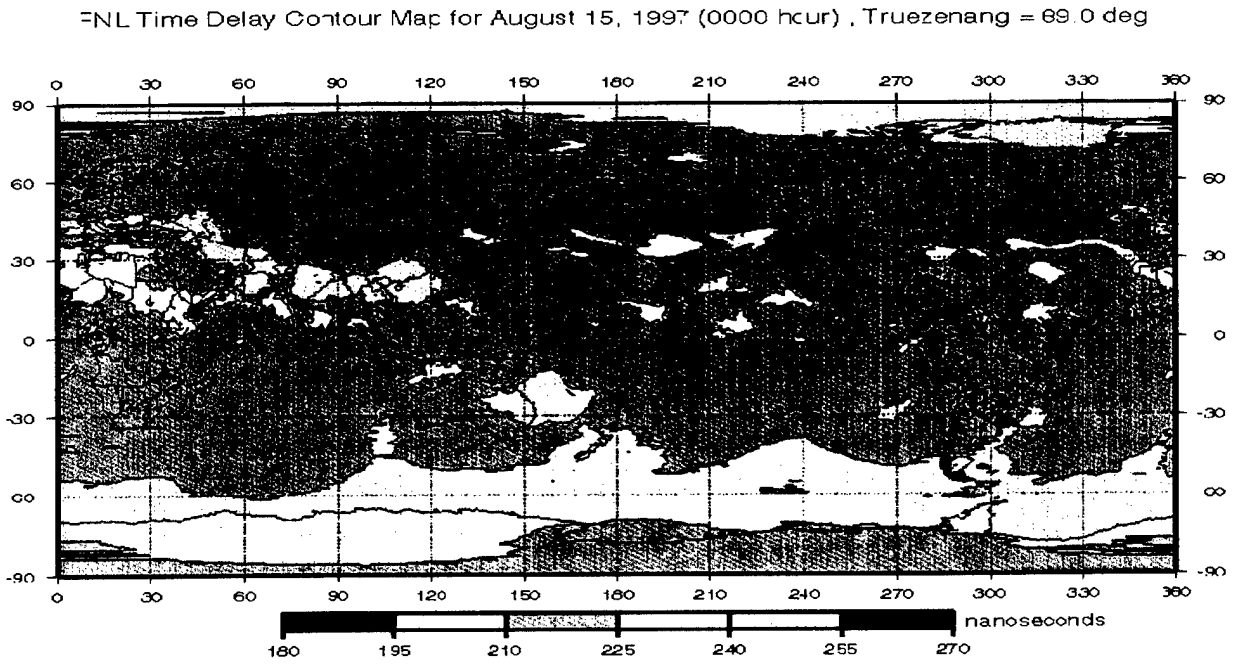

Figure 17. FNL Time Delay Contour Map for August 15, 1997 (elevation = 1.0 deg)

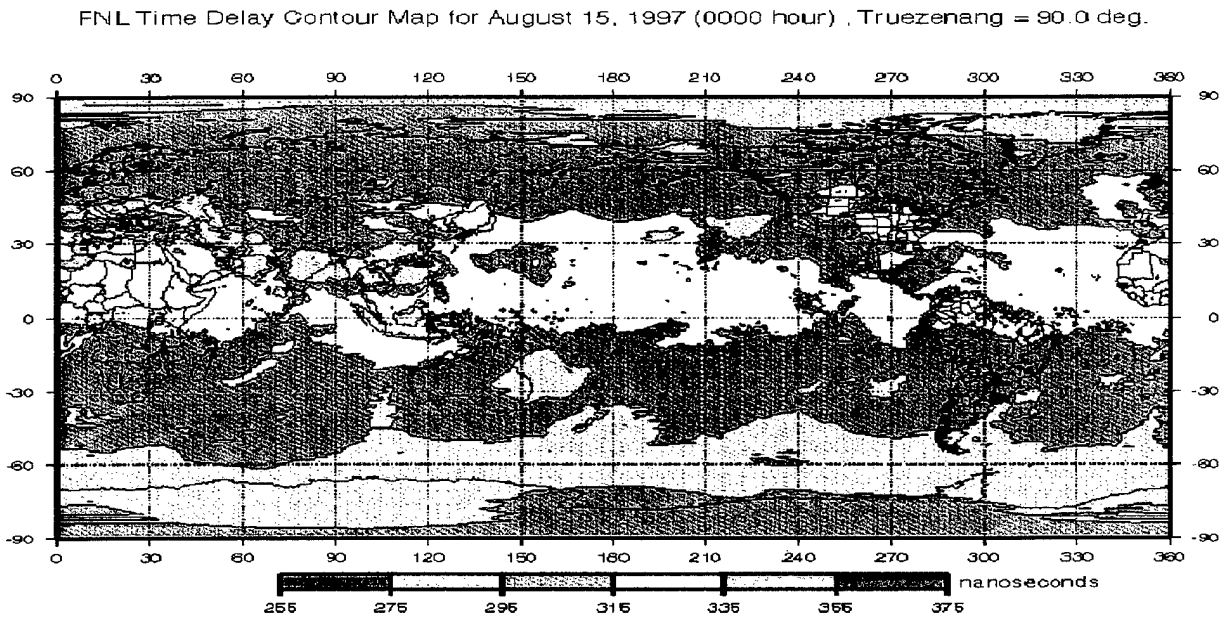

Figure 18. FNL Time Delay Contour Map for August 15, 1997 (elevation = 0.0 deg)

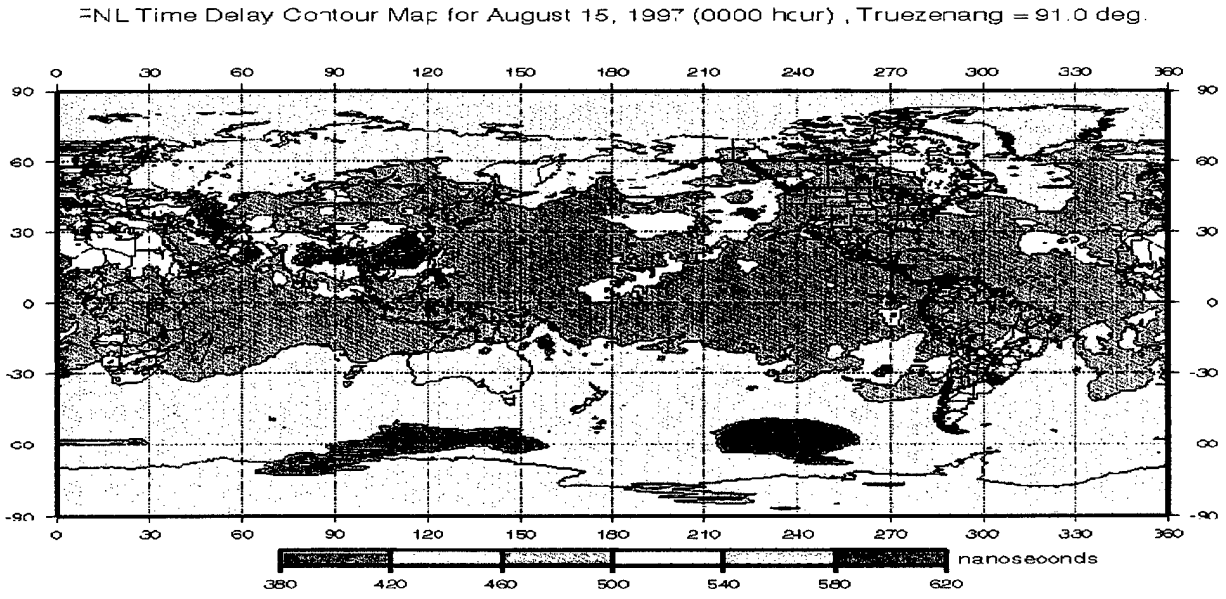

Figure 19. FNL Time Delay Contour Map for August 15, 1997 (elevation = -1.0 deg)

Table 2. Time Delay Difference between ECM and FNL for August 1997

Ecm-FNL	site1	site2	site3	site4	site6	site7	site8	Denver	Sahara	Everest	Korea
10	0.112145	0.634684	0.747452	2.298476	0.553383	0.006901	1.725603	0.670066	-0.87157	1.90248	0.138906
9	0.168462	0.73278	0.775127	2.553204	0.620586	0.057302	1.969923	0.756012	-1.03876	2.18801	0.188323
8	0.255083	0.865015	0.789958	2.872158	0.706755	0.137699	2.294398	0.867594	-1.27343	2.572711	0.26274
7	0.392762	1.051066	0.776442	3.282522	0.821161	0.270197	2.74226	1.017775	-1.617	3.111973	0.378594
6	0.62219	1.325492	0.702615	3.829715	0.979656	0.496582	3.390364	1.229296	-2.14677	3.907496	0.567903
5	1.02648	1.754952	0.497579	4.592658	1.211463	0.902377	4.384703	1.544155	-3.01551	5.156901	0.895546
4	1.790791	2.476963	-0.00224	5.722413	1.575446	1.675753	6.025358	2.047695	-4.55285	7.279324	1.503888
3	3.372076	3.802739	-1.21034	7.53964	2.20381	3.271209	8.988799	2.929759	-7.54199	11.26101	2.737856
2	7.057591	6.516651	-4.29217	10.82886	3.435598	6.923105	14.98586	4.668228	-14.0966	19.75964	5.544709
1	17.19802	12.88046	-13.0695	17.92338	6.313408	16.54542	29.0181	8.664716	-30.9659	41.35342	12.99728
0	47.57841	28.63327	-38.8679	35.37549	13.80339	43.33693	64.10278	18.60004	-77.9564	102.0162	34.22412
-1	56.76919	38.95805	-49.8654	42.22833	16.99793	55.65993	85.345	24.22603	-97.2755	124.5833	42.61741
-2	77.60822	55.05421	-70.7194	55.24509	22.90757	78.02349	119.3937	33.42997	-134.195	170.0061	58.99339
-3	105.232	74.78204	-97.4466	72.15736	30.504	106.4942	161.4889	44.90273	-181.738	229.0235	80.17029

Table 3. Angle Error Comparison August 1, 1999 for 8 sites

	site1		site2		site3		site4		site5		site6		site7		site8	
	chi	hop	chi	hop	chi	hop	chi	hop	chi	hop	chi	hop	chi	hop	chi	hop
10	-0.0049	-0.0035	0.0094	-0.0019	-0.0046	-0.0029	-0.0042	-0.0027	-0.0035	-0.0034	-0.0016	-0.0029	0.0021	-0.0028	-0.0055	-0.0029
9	-0.0055	-0.0048	0.0027	-0.0031	-0.0052	-0.0040	-0.0047	-0.0039	-0.0038	-0.0047	-0.0017	-0.0033	0.0023	-0.0039	-0.0063	-0.0033
8	-0.0063	-0.0058	0.0080	-0.0043	-0.0059	-0.0055	-0.0053	-0.0054	-0.0037	-0.0063	-0.0019	-0.0046	0.0025	-0.0053	-0.0071	-0.0049
7	-0.0073	-0.0069	0.0084	-0.0060	-0.0069	-0.0073	-0.0068	-0.0077	-0.0038	-0.0068	-0.0021	-0.0062	0.0027	-0.0070	-0.0082	-0.0064
6	-0.0086	-0.0080	0.0090	-0.0080	-0.0082	-0.0095	-0.0071	-0.0099	-0.0040	-0.0075	-0.0025	-0.0088	0.0029	-0.0090	-0.0095	-0.0085
5	-0.0107	-0.0098	0.0097	-0.0095	-0.0102	-0.0122	-0.0086	-0.0126	-0.0042	-0.0094	-0.0029	-0.0095	0.0032	-0.0126	-0.0116	-0.0121
4	-0.0133	-0.0126	0.0095	-0.0129	-0.0132	-0.0156	-0.0107	-0.0159	-0.0045	-0.0124	-0.0035	-0.0123	0.0034	-0.0159	-0.0146	-0.0154
3	-0.0194	-0.0154	0.0089	-0.0209	-0.0165	-0.0238	-0.0148	-0.0229	-0.0052	-0.0233	-0.0042	-0.0227	0.0033	-0.0230	-0.0195	-0.0229
2	-0.0305	-0.0249	0.0085	-0.0365	-0.0268	-0.0434	-0.0201	-0.0357	-0.0059	-0.0427	-0.0049	-0.0332	0.0027	-0.0371	-0.0285	-0.0394
1	-0.0597	-0.0791	0.0081	-0.0655	-0.0536	-0.0880	-0.0345	-0.0523	-0.0099	-0.0648	-0.0083	-0.0385	0.0018	-0.0488	-0.0487	-0.0576
0	-0.1421	-0.2228	-0.0071	-0.1588	-0.1237	-0.1922	-0.0828	-0.1688	-0.0373	-0.1807	-0.0382	-0.1115	-0.0037	-0.1309	-0.0980	-0.1555
-1	-0.0433	0.2161	0.0055	0.2592	-0.0382	0.2578	-0.0257	0.1465	-0.0080	0.1605	-0.0025	0.2120	0.0011	0.1977	-0.0049	0.3091
-2	-0.0159	0.1751	0.0044	0.2487	-0.0143	0.2914	-0.0110	-0.0886	-0.0029	-0.0035	-0.0027	0.0885	0.0002	0.0573	-0.0144	0.3352
-3	-0.0073	-1.1884	0.0026	-1.0286	-0.0055	-0.9185	-0.0057	-1.8435	-0.0015	-1.6885	-0.0007	-1.4416	0.0010	-1.4809	-0.0070	-0.6221

file contains hemispheric 129 by 129 stereographic grids and data on one hemisphere for approximately half a month; days one through 15, and 16 through the end of month. The raw FNL data are stored in the unpacked binary form with the header record. Each data record was composed of a 50-character header in ASCII format, followed by the binary packed data. To read the header record and extract binary data, one should decode the binary index record. To generate the FNL database of 1 degree by 1 degree high-resolution world data for the tropospheric program, one should reprocess raw FNL data. Figure 20 shows block diagram of the on-line data processing by connecting to the NOAA database to generate the database for a tropospheric exponential model program.

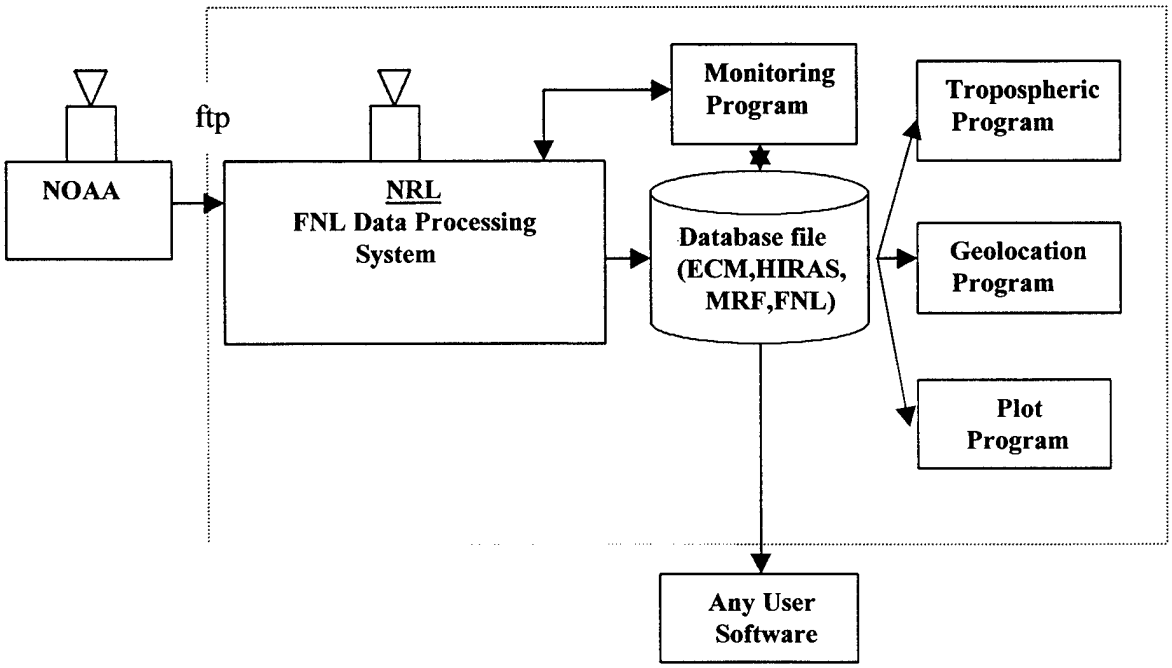

Figure 20 On-line FNL Data Processing Diagram

3.1 Unpacking FNL Database

The FNL data processing begins with the unpacking of the field and printing out the grid point which corresponds with the latitude and longitude. The program "unpack_fnl" performs the unpacking and generates the surface refractivity data from the extracted data. If the whole data set is missing, the program creates a "Missing.dat" file. This file contains information on what data is missing, and returns the number of bytes to be read. In this routine, the input data file is the raw FNL data file from NOAA. This routine passes the record number and the temporary output file name to store unpacked data for each record number as input parameters. The array filename is used to generate the name of the selected record. The following is an example of a relation between the record number and the filename.

rec 1 = hour 0000 day 1 ------- fnl_month_01_year_00.final
rec 2 = hour 0600 day 1 ------- fnl_month_01_year_06.final
rec 3 = hour 1200 day 1
rec 4 = hour 1800 day 1
rec 5 = hour 0000 day 2 ------ fnl_month_02_year_00.final
rec 6 = hour 0600 day 2 ------ fnl_month_02_year_06.final

According to the record number, the routine saves data in the memory buffer. Then, reads the raw unpacked data file to create the output data file. One buffer contains 14 different levels of data based on different pressure from surface to 20 mb at approximately 27 km height. Using the iteration loop, each layer data is extracted from the buffer. The output file produces a 3,261,636 byte binary file that contains a 129 by 129 stereographic grid of the unpacked atmospheric data. Each grid is 14 bytes in size as shown in Figure 21. The first 4 bytes contain pressure data. The next 2 bytes contain temperature data. The next 2 bytes contain relative humidity data. The next 2 bytes contain surface refractivity data. The last 4 bytes contain reference height data.

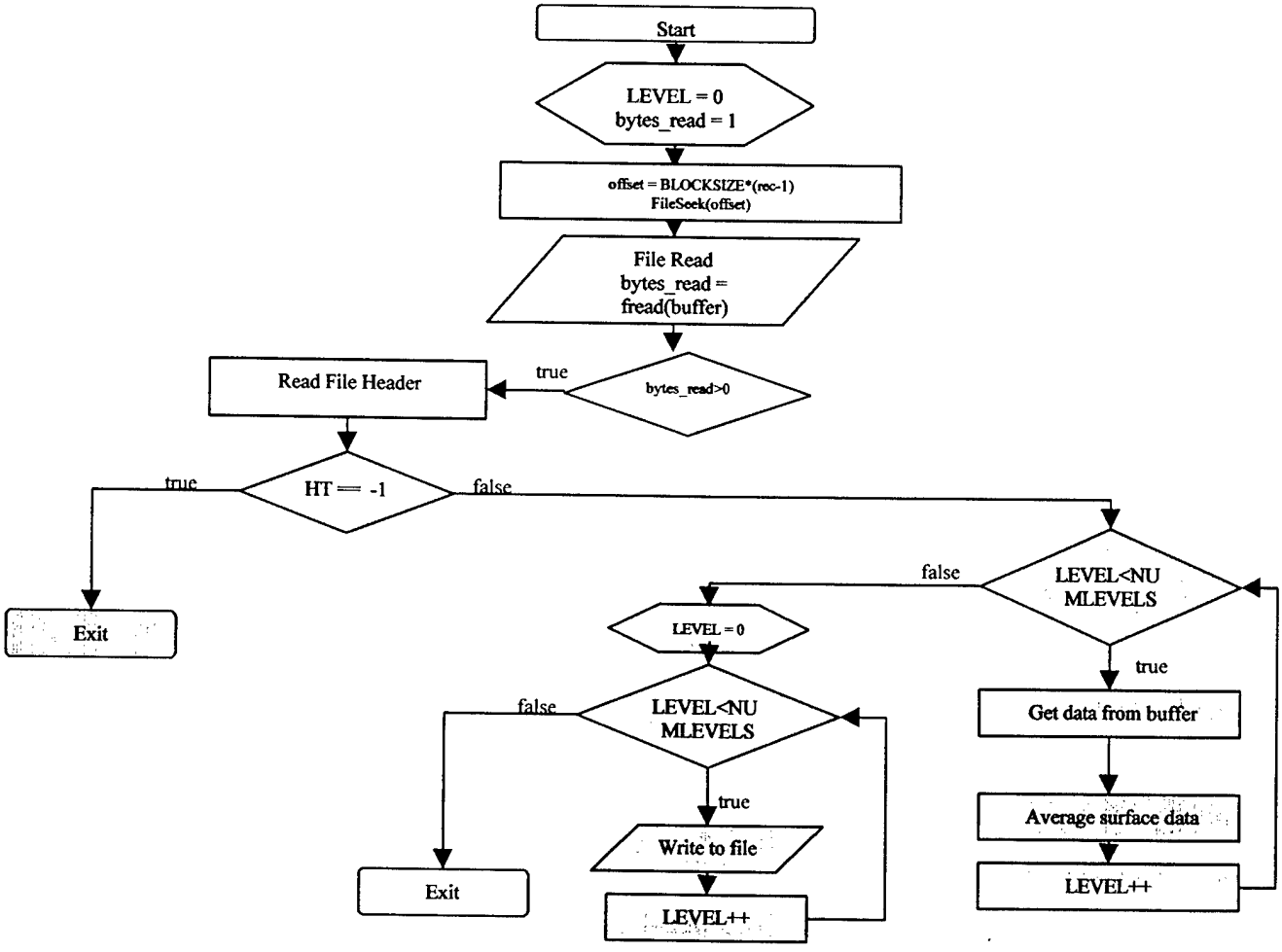

Figure 21. Unpacking Processing Diagram

3.2 Merging Processing

There is no latitude, longitude, and surface height information in the new unpacked FNL data file. We connect to the NOAA Air Resource Laboratory in Maryland to get the location information for 129-by-129 polar stereographic grids. They send two northern and southern hemispheric data sets. We generate a new file that merges the 129-by-129 latitude and longitude data with the atmospheric data. This merging program creates new temporary binary data files that merge latitude and longitude for each grid. Each grid block size of a new binary data file is 22 bytes as shown in Figure 22. The first 4 bytes are for latitude data and the next 4 bytes for longitude data. The next 4 bytes are for pressure data and the next 2 bytes for temperature data. The next 2 bytes are for relative humidity data and the next 2 bytes for surface refractivity data. The last 4 bytes contain reference height data.

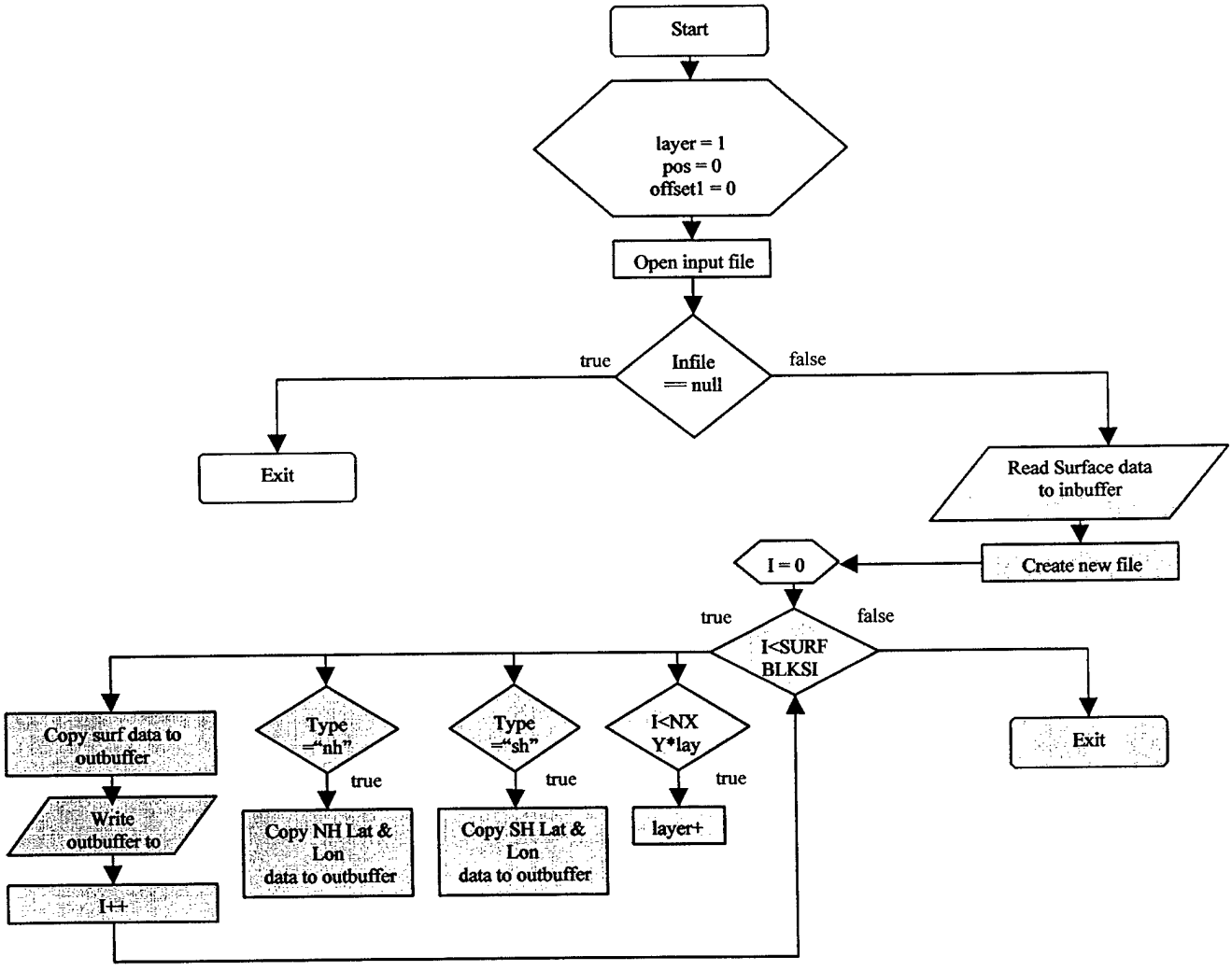

Figure. 22 Merge Data Processing Diagram

3.3 Calculating Reference Height

The tropospheric exponential model program needs a reference height for each grid as a scale factor. The newly created file contains latitude, longitude, and atmospheric data to generate a new binary file with reference height derived from atmospheric data. To determine the reference height for each grid, a simple linear interpolation method has been adopted. Given the refractivity/height pairs h_1/n_1 and h_2/n_2, we desire to determine the reference height h_0 at refractivity n_0 (see Figure 23).

Note that,

$$\log h_2 = m \log n_2 + b \tag{1}$$

And

$$\log h_1 = m \log n_1 + b \tag{2}$$

Solving for m and b,

$$m = \frac{\log[h_1 / h_2]}{\log[n_1 / n_2]} \tag{3}$$

$$b = \log h_2 - \log h_1 \tag{4}$$

The reference height h_0 at the refractivity n_0 is then found from

$$\log h_0 = m \log n_0 + b \tag{5}$$

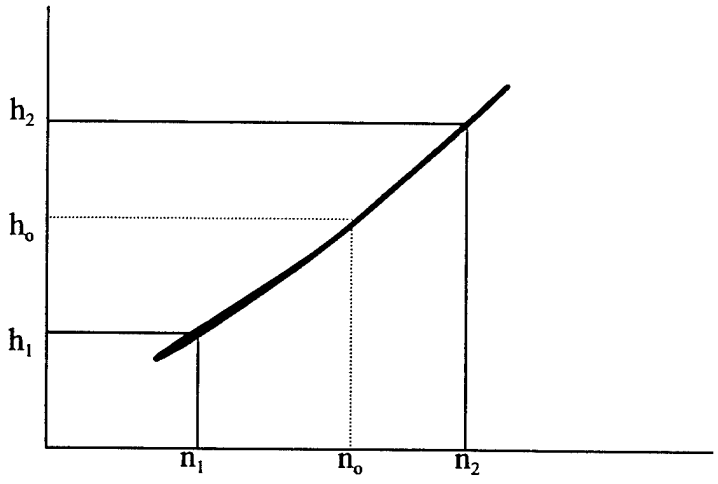

Figure 23. Interpolation Method

The return value of this routine points to the new output file. Each grid block size of the output file is 22 bytes. The first 4 bytes are for latitude data and the next 4 bytes for longitude data. The next 4 bytes are for pressure data and the next 2 bytes for temperature data. The next 2 bytes are for relative humidity data and the next 2 bytes for surface refractivity data. The last 4 bytes contain reference height data. Figure 24 shows the diagram of calculating reference height.

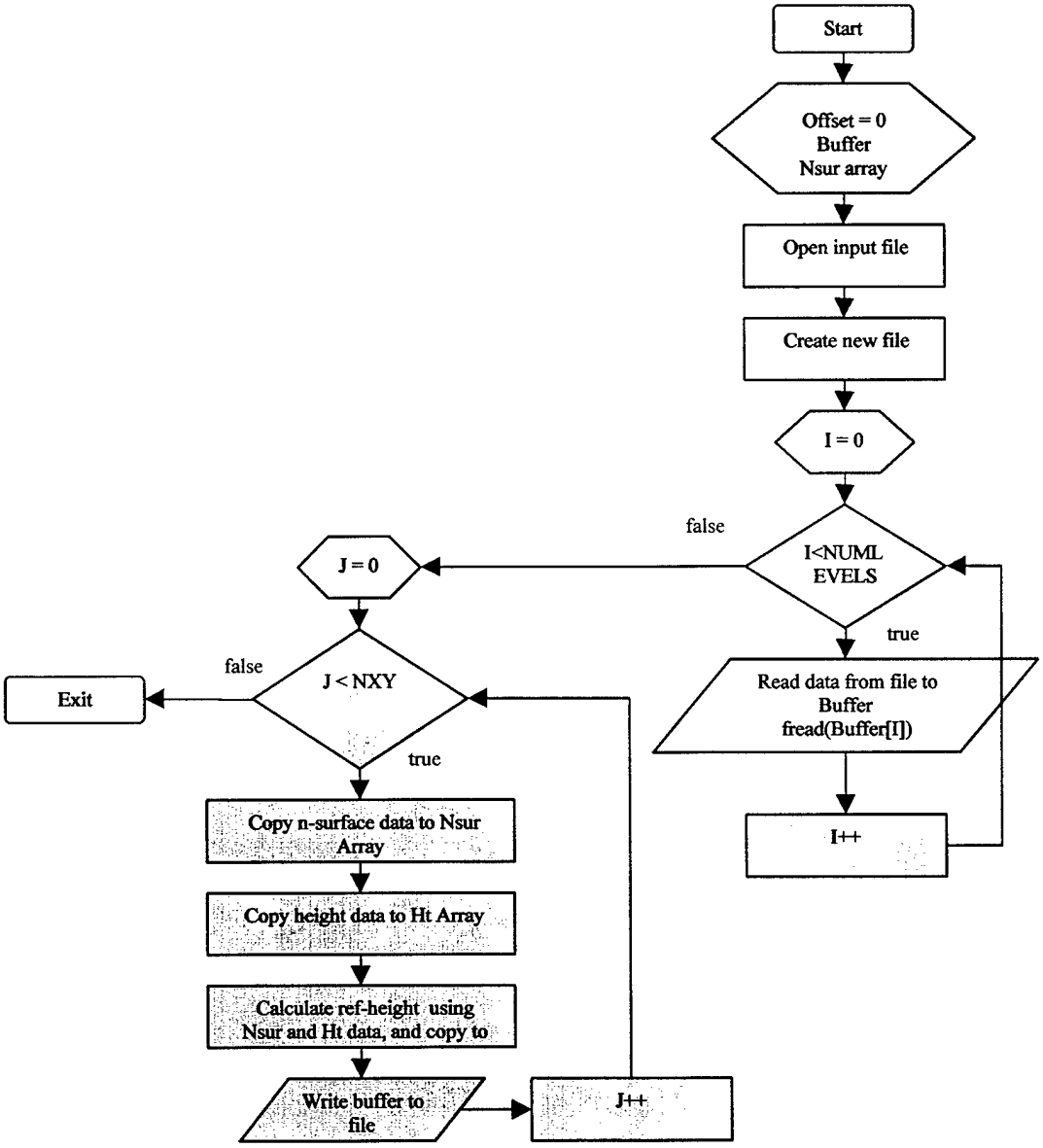

Figure 24. Calculating Reference Height Diagram

3.4 Averaging Atmospheric Data

There are more than 2 information blocks at the same grid when the FNL data is reprocessed to 1 degree by 1 degree for the tropospheric program. We use the newly created and averaged atmospheric data when grid numbers of the same value intersect. A new binary file is created which contains the calculated grid numbers and averaged atmospheric data. All data in the file is sorted in ascending order according to the grid number. The binary file data is sorted by using a binary tree sorting algorithm. A binary tree is a hierarchical structure based on a modified form of a linked list, which is request-and-release memory from/to the operating system as required by the program at a run-time. Each node in the binary tree maintains two further node pointers, known as 'left' and 'right', which point to the left and the right sub-trees of that node. Absent sub-trees are marked by a NULL valued left or right within their corresponding node. A node with neither left nor right sub-tree is known as a leaf node, while the node at the top of the tree is called the root node. This binary tree sorting algorithm has the ability to rapidly search and sort the data. Also, it is easy to insert and delete data into memory. The data structure of this binary tree is

```
Structure    BinNode {
             Int          item;
             Struct       BinNode   *left;
             Struct       BinNode   *right; }
```

The integer item presents the grid number. The grid number is greater than the grid number of the other node, then it goes to the right binary node. It does not go to the left node to sort the grid number for random data file. According to the sorted grid number, the data in the memory buffer copies into the record array to create an output file. The output file of this routine contains grid number data instead of latitude and longitude data for each grid. Each grid block size of output file is 16 bytes. The first 2 bytes are for grid number data and the next 4 bytes for pressure data. The next 2 bytes are for temperature data and the next 2 bytes for relative humidity data. The next 2 bytes are for surface refractivity data and the last 4 bytes for reference height data. Figure 25 shows the average stratified method data processing diagram.

3.5 Missing Data

Once data has gone through the averaging atmospheric data process, it is then highly probable that there may be some missing data. All 64,800 grid numbers may not have been generated. To fill these missing grid numbers with their corresponding linear interpolated atmospheric data, linear interpolation techniques were applied. This interpolation routine checks and generates a final binary file by the grid number with their corresponding linear interpolated atmospheric data. In this routine, we used a

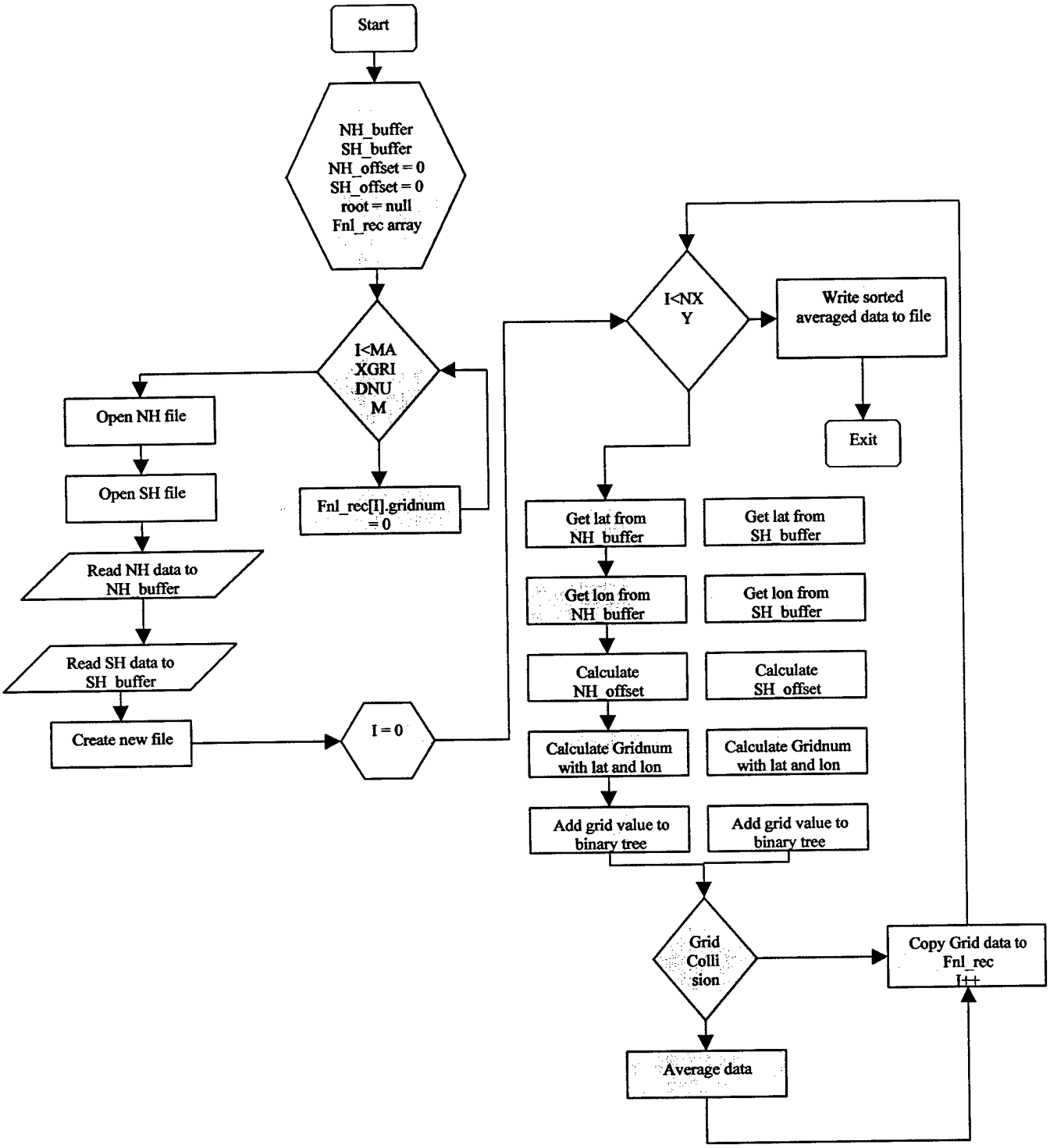

Figure 25. Average Stratified Method Data Processing Diagram

double linked-list algorithm for the missing data point. The first two nodes (head and tail) are initialized and invoked into node. If the difference of the grid number into the head and tail node is greater than one, missing data points exist in two point nodes. This routine creates nodes as much as the difference between the head and tail grid number and fill missing data using the linear interpolation method into the newly created node. The final grid block size of each output file is 16 bytes. The first 2 bytes are for the grid number data and the next 4 bytes for pressure data. The next 2 bytes are for temperature data and the next 2 bytes for relative humidity data. The next 2 bytes are for surface refractivity data and the last 4 bytes for reference height data. Figure 26 shows the additional missing data processing diagram.

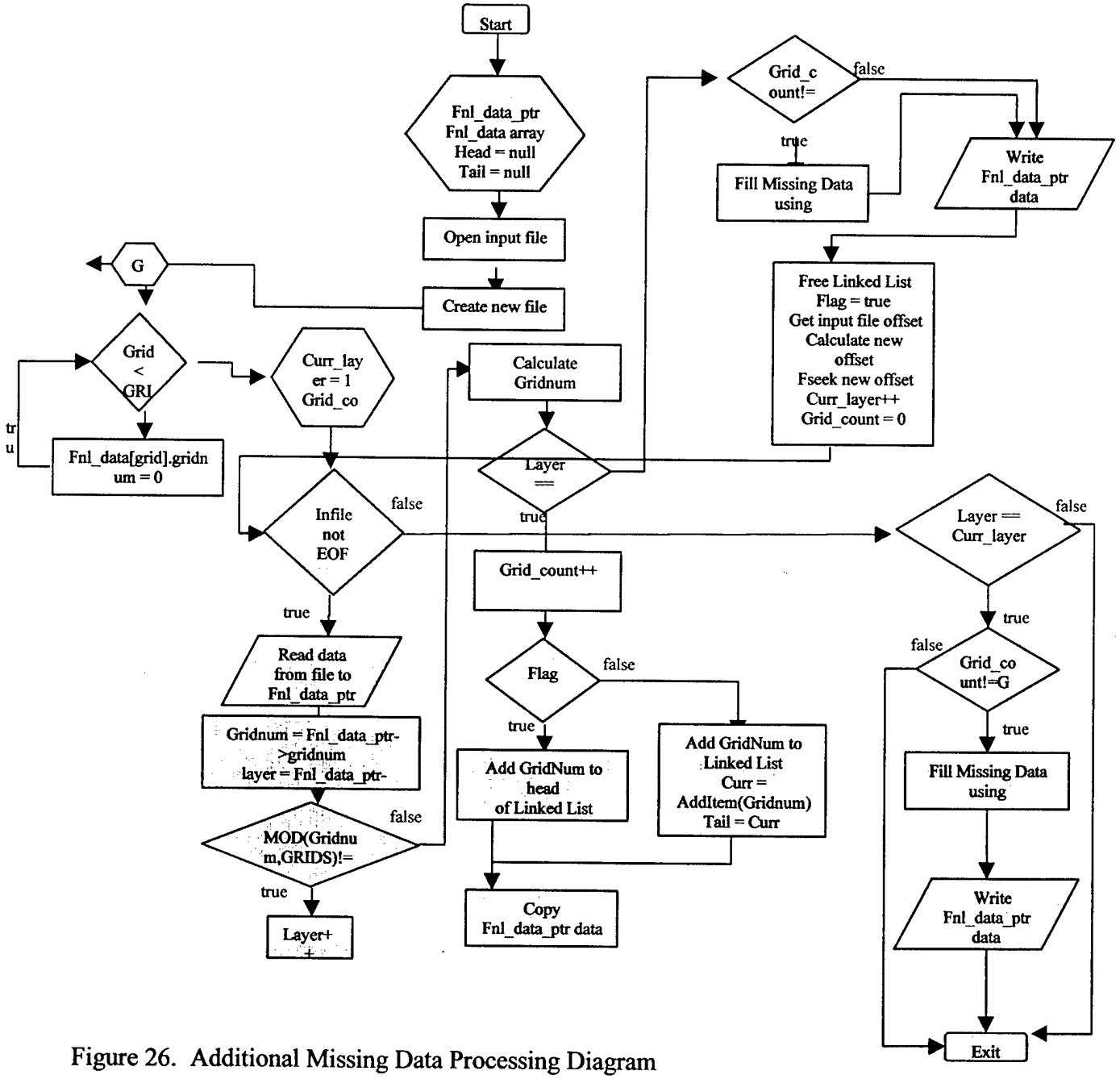

Figure 26. Additional Missing Data Processing Diagram

3.6 Automatic Process

A shell script was developed for the execution of each routine to process raw NOAA FNL binary files automatically. There are two input options to execute the shell script. One automatically calculates how many records are available to generate the final FNL data file. The other processes the particular record only. This routine processes the routine 3.1 through routine 3.5 automatically with the input record parameter to create the final output binary data files.

4. Geolocation Accuracy Measure with Tropospheric Delay

The geolocation of a radio transmitter has a wide variety of applications. One example is to locate an emergency radio source for ship or aircraft rescue. Another is to find the position of an interference source that interferes with satellite operations.

The geolocation measure of the radio transmitter is based mainly on techniques which relate to one or a combination of frequency and time information. The set of delays, or time difference of arrival (TDOA), associated with each of the source wave fronts between the receivers can be used to determine the source location by solving a nonlinear or linear system equation. In this report, we use TDOA measurements in which a propagation time for the uplink signal through a particular satellite is compared with an adjacent satellite. Given that the position of two spacecraft relative to the receiving station is precisely known, the difference between the time of arrival over the two different paths will localize the uplink transmitter location to a curve on the surface of the Earth. Since the TDOA technique described only localizes the position of the uplink transmitter to a curve on the surface of the Earth, some additional techniques are required to resolve the ambiguity. Initially, it was thought that the ambiguity could be resolved by making the third spacecraft to form another signal path pair. Then, the position of the uplink in question could be determined by finding the intersections of the two resulting arcs. Figure 27 presents a two dimensional view of geometry pertinent to the TDOA technique. The position of the two satellites, the location of the TDOA site, and the distance from the satellites to the TDOA receiver site are known. The unknowns are the two remaining distances from each of the satellites to the unknown uplink station.

If the receiver site has two antennas connected to two receiving systems which can simultaneously monitor the signal through each satellite, a receive time delay between the two paths can be measured. Given this delay along with the knowledge of the speed of the signal propagation through space and the equivalent distance of any unnoticeable signal processing time, the difference in path distances may be deduced. Subtracting out the known downlink distance and any other system offsets from the satellites to the TDOA receiver site leaves the remaining differential distance between the two unknown uplink distances.

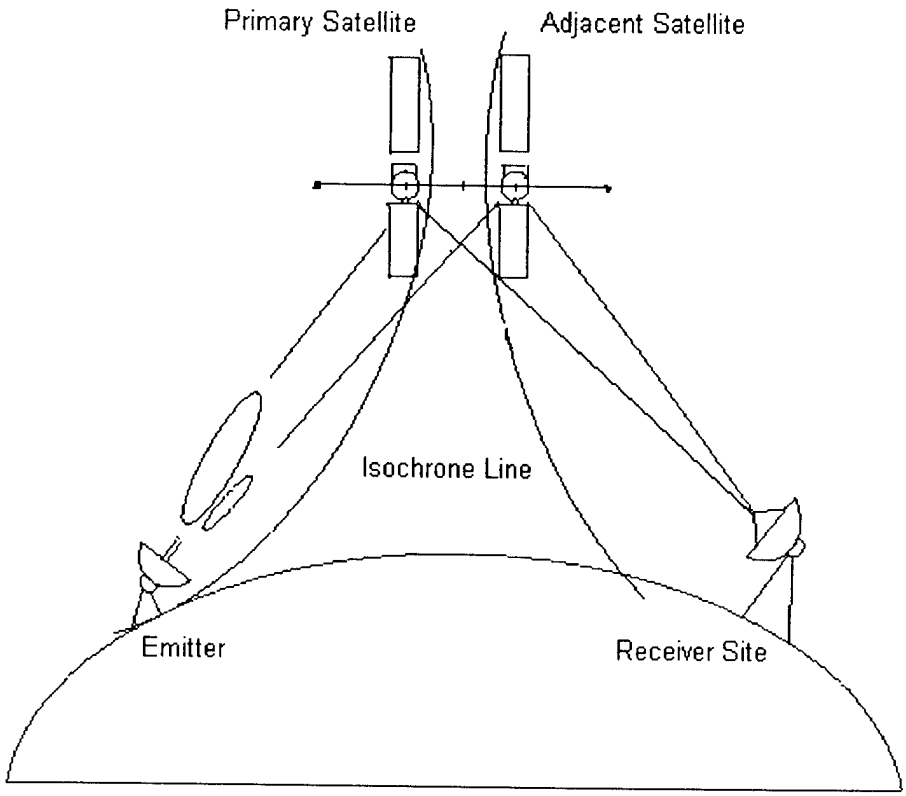

Figure 27. Two-Dimensional TDOA Geometry (Isochrone Intersection)

4.1 Covariance and SMA/SMI Estimation

The components of an n-dimensional vector x that is to be estimated are the position.

$$x = [\, x_1, x_2, \ldots, x_n] \qquad (6)$$

A set of N measurements y_i, i= 1, 2, ... n is collected at various positions. In the absence of random measurement errors, y_i is equal to a known function f(x). In the presence of additive errors,

$$y_i = f_i(x) + v_i, \quad i = 1,2, \ldots, n \qquad (7)$$

These n-equations can be written as a single equation for n-dimensional column vectors;

$$y = f(x) + v \qquad (8)$$

where v is measurement noise, the estimate of x is a matter of minimizing a cost function such as the weighted sum of squared residuals,

$$Q(x) = e(x)^t \, W \, e(x) \qquad (9)$$

where $e(x) = y - f(x)$ and t is the transpose of the vector e(x).

The weight matrix is the inverse of the covariance matrix of noise measurements. In general, f(x) is a nonlinear vector function. To determine a reasonably simple estimator, f(x) can be linearized by expanding it in a Taylor series about a reference point specified by the vector x_0 and retaining the first two terms; that is, we use

$$f(x) = f(x_0) + A\,(x - x_0) \qquad (10)$$

Where x and x_0 are n x 1 column vectors and A is the n x n matrix of derivatives evaluated at x_0:

$$A = \begin{bmatrix} \left.\frac{\partial f_1}{\partial x_1}\right|_{x=x_o} & \cdots & \left.\frac{\partial f_1}{\partial x_n}\right|_{x=x_o} \\ \left.\frac{\partial f_n}{\partial x_1}\right|_{x=x_o} & & \left.\frac{\partial f_n}{\partial x_n}\right|_{x=x_o} \end{bmatrix} \qquad (11)$$

Each row of this matrix is the gradient vector one of the components of function f(x). The vector x_0 could be an estimate of x determined from a previous iteration of the estimation procedure or based on prior information. It is assumed in the subsequent analysis that x_0 is sufficiently close to x that the equation $f(x) = f(x_o) + A(x-x_o)$ is an accurate approximation. Combining equation (9) and equation (10) gives

$$Q(x) = (e_l - Ax)^t W^{-1} (e_l - Ax) \qquad (12)$$

where $e_l = e - f(x_0) + Ax_0$.

To determine the necessary condition for the estimator x that minimizes Q(x), we calculate the gradient of Q(x), defined by

$$\frac{\partial}{\partial x} Q(x) = \left[\frac{\partial Q}{\partial x_1} \; \frac{\partial Q}{\partial x_2} \; \cdots \; \frac{\partial Q}{\partial x_n} \right] \qquad (13)$$

And then solve for x such that

$$\frac{\partial}{\partial x_i} Q(x) = 0 \tag{14}$$

From its definition, W is a symmetric matrix. Therefore

$$\frac{\partial}{\partial x_i} Q(x) = 2A^t WA\hat{x} - 2A^t W \tag{15}$$

We assume that the matrix A^tWA is non-singular. Thus the solution is

$$\hat{x} = (A^tWA)^{-1}A^tWe_i = x_o + (A^tWA)^{-1}A^tWe \tag{16}$$

For all cases, the covariance matrix $[A^tWA]^{-1}$ at the final step gives the statistics of final position estimates. For the estimator of a two-dimensional vector, such as position coordinates on the surface of the Earth, the bivariate covariance matrix can be expressed as

$$P = \begin{bmatrix} \sigma_1^2 & \sigma_{12} \\ \sigma_{12} & \sigma_2^2 \end{bmatrix} \tag{17}$$

and with the assumption that the error distribution is a Gaussian, the parameter of error ellipse with a = semi-major axis and b = semi-minor axis is determined by

$$a^2 = \frac{2\left\{\sigma_1^2\sigma_2^2 - \sigma_{12}^2\right\}}{\left\{\sigma_1^2 + \sigma_2^2 - \left[\left(\sigma_1^2 - \sigma_2^2\right)^2 + 4\sigma_{12}^2\right]^{1/2}\right\}} \tag{18}$$

$$b^2 = \frac{2\left\{\sigma_1^2\sigma_2^2 - \sigma_{12}^2\right\}}{\left\{\sigma_1^2 + \sigma_2^2 + \left[\left(\sigma_1^2 - \sigma_2^2\right)^2 + 4\sigma_{12}^2\right]^{1/2}\right\}} \tag{19}$$

The axis direction is

$$\theta = \frac{1}{2}\tan^{-1}\left(\frac{2\sigma_{12}}{\sigma_1^2 - \sigma_2^3}\right) \tag{20}$$

4.2 Geolocation Measure using TDOA

The geolocation program uses time difference of arrival (TDOA) measurements as the measurement parameter for its estimation process. Thus, the estimation problem becomes a problem of determining the functional relationship between TDOA and the estimation parameters. Given the range distance from the emitter to the spacecraft, R(t) and the atmospheric delay $d_{atm}(t)$, the TDOA is given by

$$\tau(x,t) = (1/c)\, R(t) + d_{atm}(t) + \varepsilon \qquad (21)$$

where

$$R(t) = \| r(t) \| = (r^t r)^{1/2} \qquad (22)$$
$$r = s - l$$

with s representing the position of spacecraft, and l the emitter location. Then, the calculated TDOA between spacecraft 1 and 2 is given by

$$f_{12}(x) = \tau_2(t_2) - \tau_1(t_1)$$

$$= (1/c)[R_2(t_2) - R_1(t_1)] + d_{atm,2}(t_2) - d_{atm,1}(t_1) \qquad (23)$$

4.3 Analysis Result

The TDOA analysis for an emitter geolocation is required to validate the accuracy of the model due to the change of velocity for the radio frequency (RF) wave with respect to the refractivity variation in the troposphere region. The precision geolocation algorithms of the current Ramrod system use an approximation of the Hopfield model that produces significant errors in computing the time delay at low elevation angles (less than 3 degrees). The Hopfield model applied zero time delay at negative elevation angle to the spacecraft. The exponential model (Choi model) has used the historical climatology weather data and an improved algorithm to provide a more accurate time delay profile. The time delay profile of the exponential model (Choi model) would provide better location and reduce the uncertainty associated with those inferred emitter positions. The geolocation program has been developed to allow the operator to choose which of the two troposphere models (Hopfield or Choi model) should be adopted for the process of a particular signal set. A 100 nanoseconds difference between the Hopfield and Choi model at low elevation angles suggests that a significant correction may be able to be made in the low elevation TDOA. The Choi model used temporal and meteorological data. We used different atmospheric factor, covariance time delay, and atmospheric delay instead of

constant values as for the Hopfield model when applied to the current Ramrod system. We observed that the Choi model improved the miss distance and the uncertainty approximately 50% in comparison with the current Hopfield model. This report covered the results of the emitter geolocation data sets for six different events collected in January 21, 1998. Figure 28 depicts the collected benchmark data format.

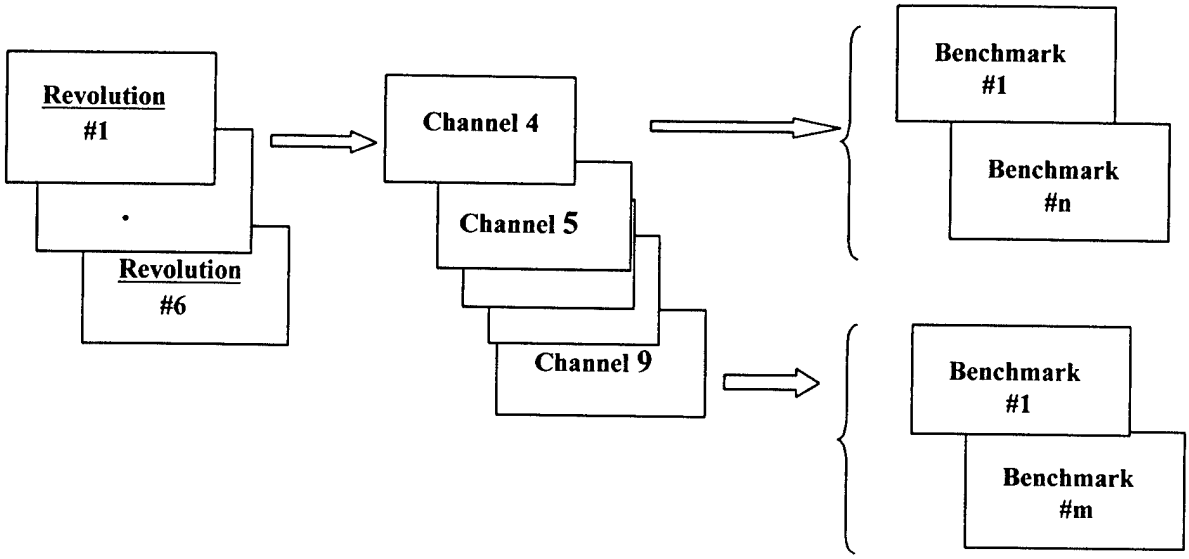

Total 2034 benchmarks

Figure 28. Collected Benchmark Data Format

These events provide a typical collection of signals on benchmark channels. The data sets associated with each event contain the scan files and signal files associated with the events. The scan data included the initial location of geolocation program, TOA of each spacecraft, and TDOA associated with each pair of the spacecraft. The data set is applied to the geolocation program for the results of miss distance and the uncertainty of the benchmark emitter position. The actual benchmark emitter location is used as an initial location instead of the estimated location. The output (Miss distance, SMA, and SMI) of the geolocation program is iterated only once for the above scan data set. The geolocation program read the initial benchmark location, associated ephemeris data, and output the position of each spacecraft. The range from the benchmark to the spacecraft was computed and the residual error between observation and measurement time delay produced. The tropospheric propagation delay was implemented by computing residual errors and applying a geolocation algorithm to generate miss distance and uncertainty.

We examined the relationship among benchmark parameters to see if the Choi model had a predictably favorable impact on the signal geolocation. Since benchmark locations are known, the benchmark miss distance is a powerful indicator of the system

model accuracy. We would expect that the Choi model would lead to a reduced miss distance at low elevation angle signals. The next parameters of interest were SMA and SMI uncertainty which reflect the statistical uncertainty in the position solution. Figures 29 through 31 show SMA, SMI, and miss distances of the 150 benchmark signals for one channel of three different events. These figures show that the Choi model appears to reduce miss distances and uncertainties more than the Hopfield model. In Figures 29 and 30, one can find that some SMA parameters (Choi Model) of certain benchmark signals are greater than those of the Hopfield SMA. But the miss distance (Choi model) of that benchmark is less than the Hopfield miss distance. These cases show that the ellipse error bound using the Hopfield model never covers a benchmark location. However, the ellipse error boundary using the Choi model is greater than that of the Hopfield, always covering the benchmark location. Figure 32 shows those cases.

Figure 33 shows three different ellipse errors probability (EEP 95%) plots for different elevation angle ranges in one benchmark scan data set. In Figure 33.1, the ellipse indicates the case of the elevation angle from 9.08 degrees to 18.48 degrees. The miss distance of the Choi model is 1,166.20 feet and the Hopfield model 3,570.85 feet. In Figure 33.2, the ellipse shows the case of the elevation angle from 13.47 degrees to 31.49 degrees and then decreased to 15.66 degrees. The miss distance of the Choi model is 355.17 feet and the Hopfield model 667.20 feet. In Figure 33.3, the ellipse presents the case of the elevation angle from 17.77 degrees to negative 0.66 degrees. The miss distance of the Choi model is 3,428.26 feet and the Hopfield model 4,406.05 feet. Figure 33.4 shows six ellipses in the same scale. In this plot, precise geolocation is usually associated with the scan segment received at the high elevation angle from the emitter to the spacecraft.

The geolocation accuracy of the Choi tropospheric model is improved approximately 50% of the uncertainty as reflected in the SMA and the miss distance. We observed that the Choi tropospheric time delay model appears to improve geolocation accuracy of the benchmark miss distance and reduce in the SMA (uncertainty in the calculated position). We can infer from these six different event data sets that the Choi tropospheric model reflects a significant improvement in the benchmark miss distances and uncertainties (SMA and SMI).

5. Conclusion and Recommendation

There are two major dominant factors in tropospheric RF propagation angular bending and time delay. These measurement errors can readily be corrected by means of ray-bending compensation through refractive profiles or ray tracing algorithms that can be computed on real or near real time weather data such as surface temperature, pressure, and relative humidity or dew point. The proposed model (Choi tropospheric model) can generate errors of both range and time delay and angle of arrival in near real-time and real-time for calibration of tracking, navigation, and satellite location in the world. This enhancement will save time and reduce risk in locating the mission target and search-and

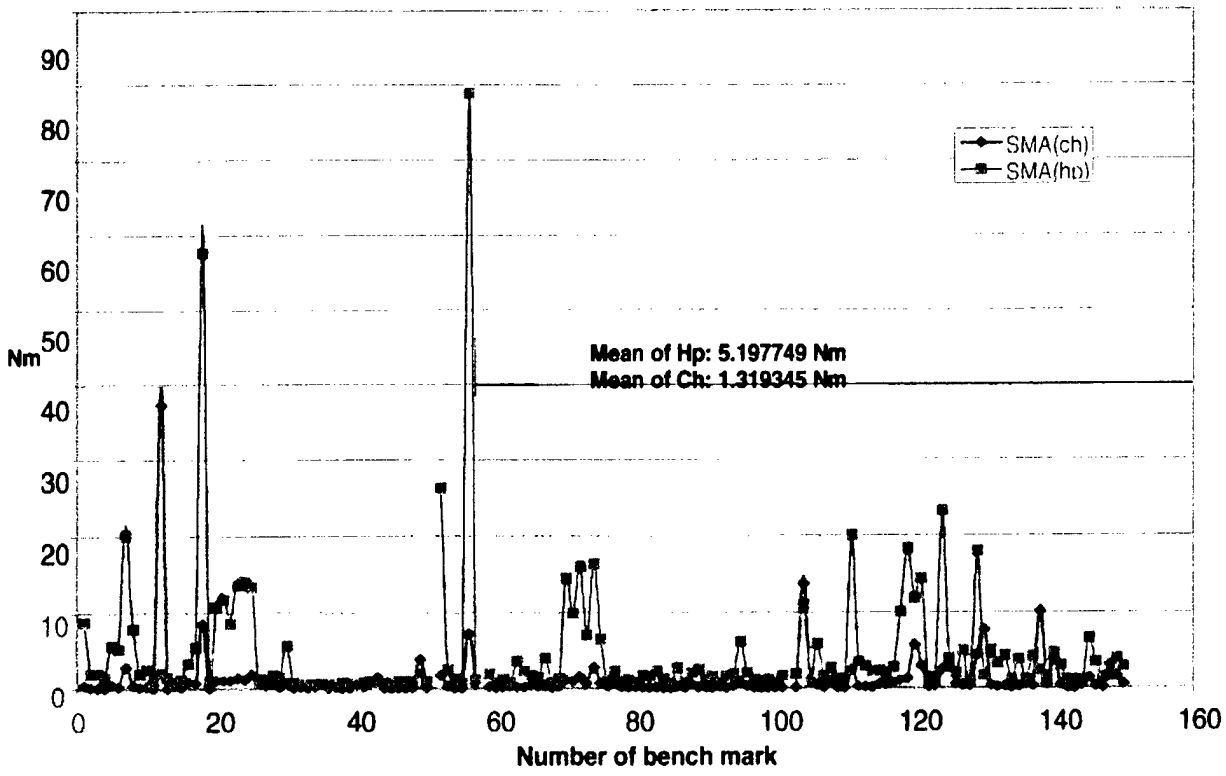

Figure 29 SMA for one channel of three different events

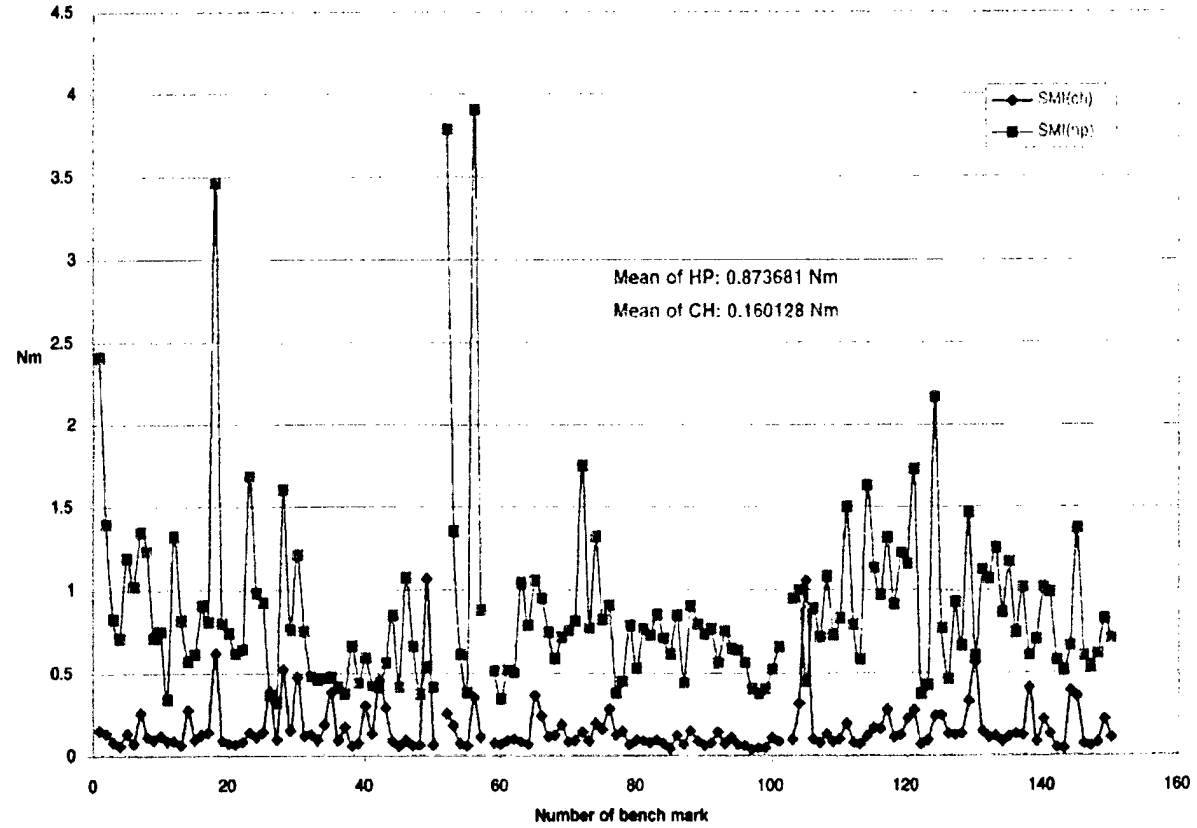

Figure 30 SMI for one channel of three different events

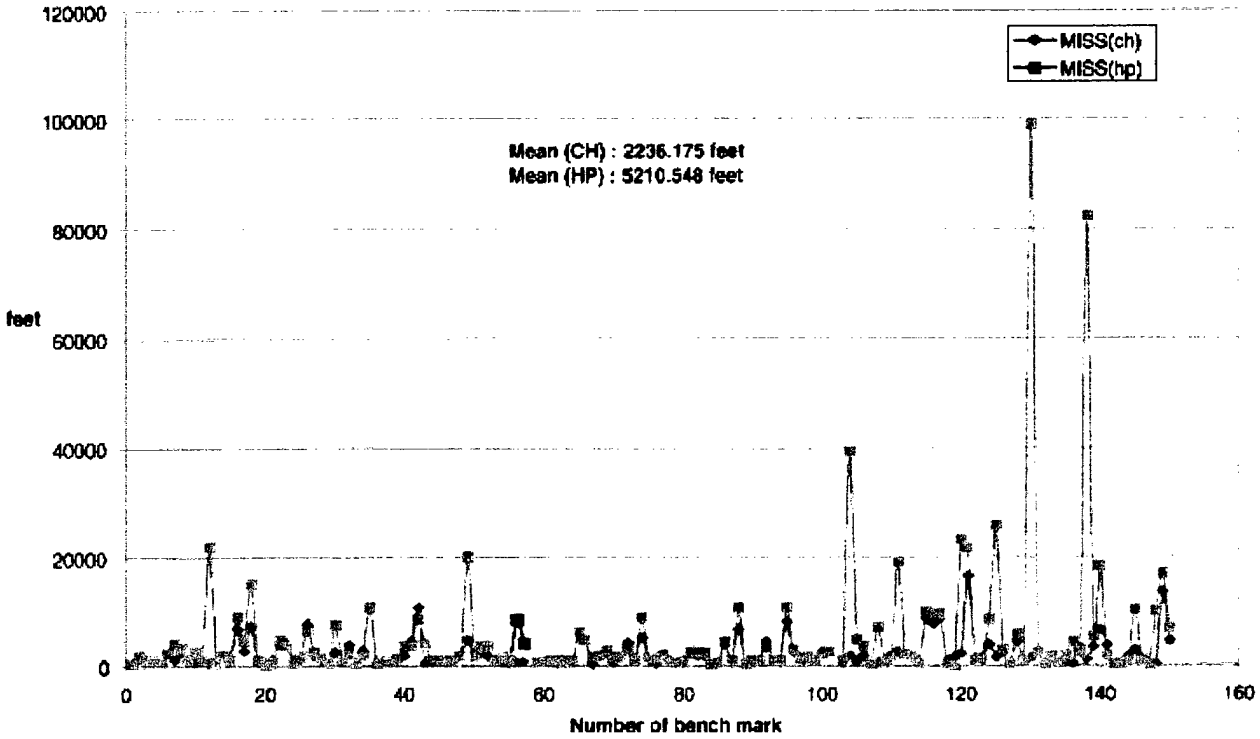

Figure 31 Miss distance for one channel of three different events

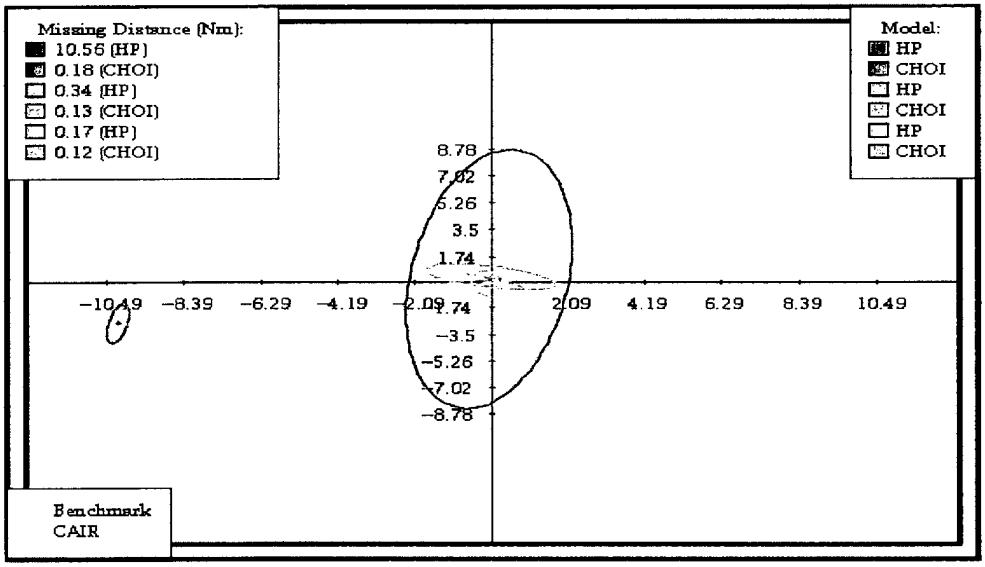

Figure 32 Error ellipse plot for benchmark CAIR

Figure 33.1

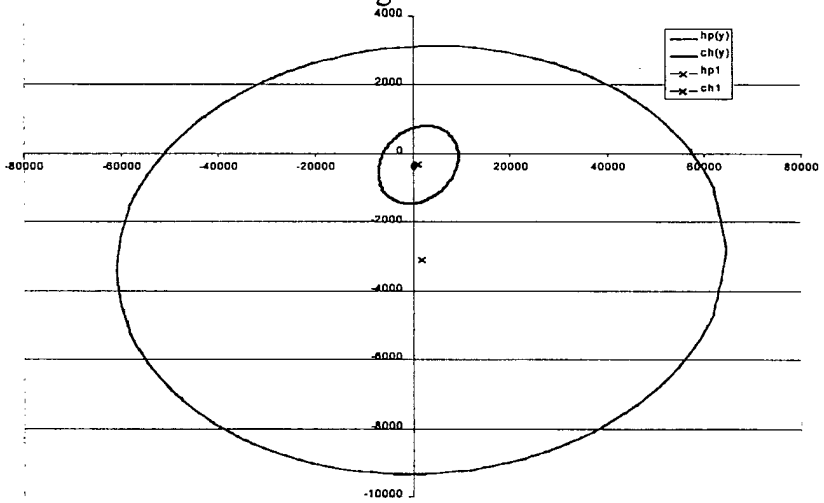

Figure 33.2

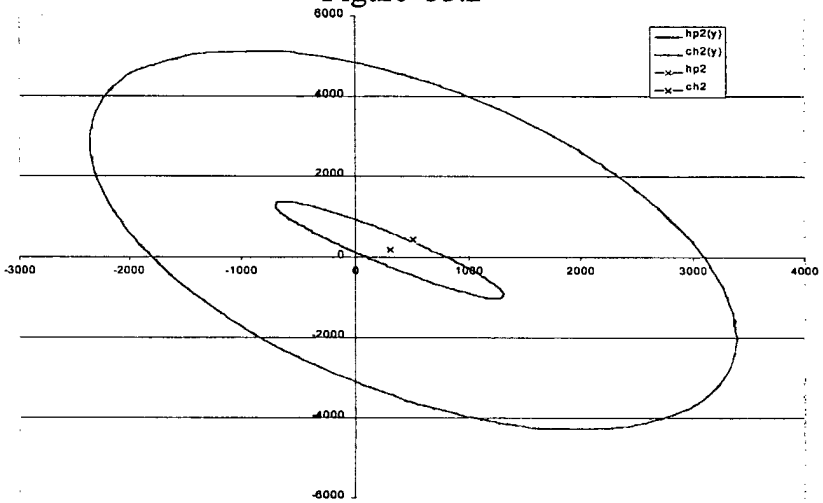

Figure 33.3

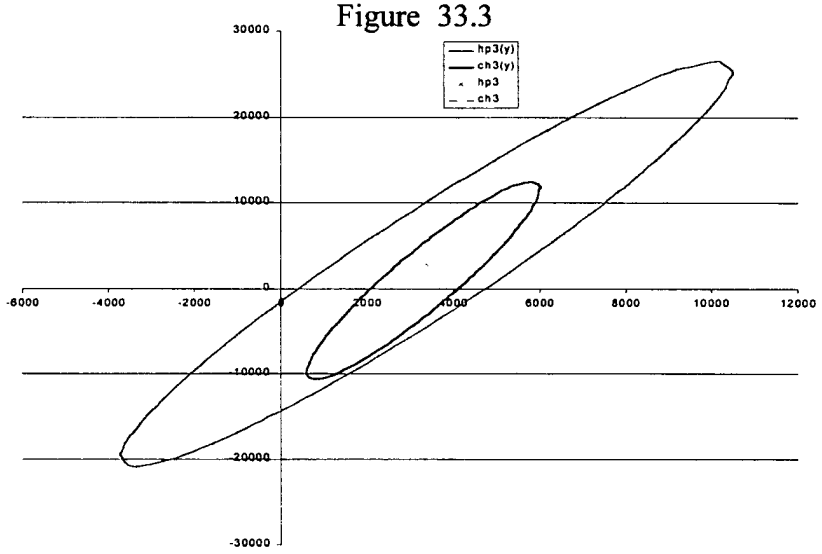

Figure 33.4

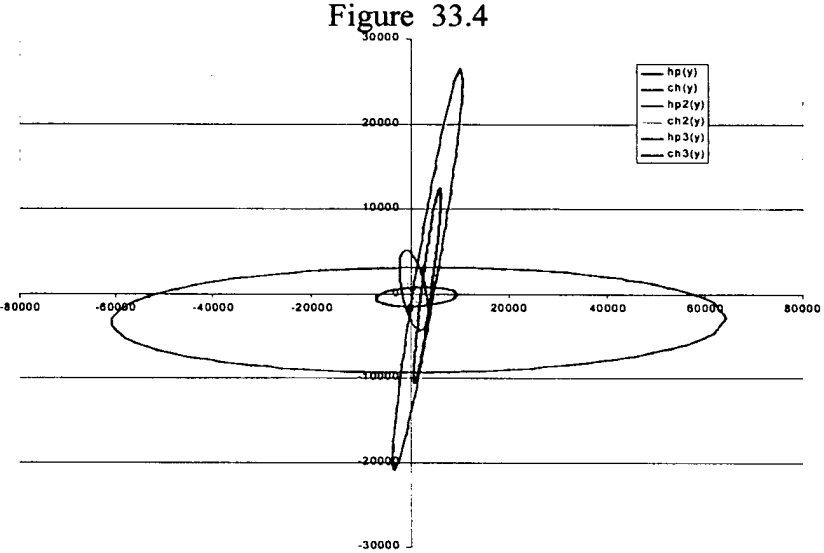

Figure 33. Three Different EEPs for Different Elevation Ranges

rescue (SAR) mission for both military and commercial applications. The Choi model is currently in the process of operational test and evaluation in MRC and IAEP.

The Choi tropospheric propagation model clearly affects the precision geolocation process. Geolocation accuracy of benchmarks is improved approximately more than 50% of the time with miss distance, SMA, and SMI. Particularly, we would expect that the Choi tropospheric model would lead to reduce miss distance and cover the benchmark location in the lower elevation signals. More detailed examination of the scan data and emitter geometry may help improve more accuracy of geolocation based on the model.

For continuing accuracy improvement, several new tasks are planned to implement a total atmospheric model (tropospheric and ionospheric). The following tasks will be studied in FY2000.

1) Test and statistical analysis of geolocation accuracy improvement using more than 1000 benchmarks signal data.
2) Examine isochrone correction for geolocation using TDOA measurements.
3) Develop a general atmospheric model by combining tropospheric and ionospheric propagation characteristics.
4) Develop a frequency dependency characteristic measurement in the tropospheric region.
5) Develop a tropospheric model for the aircraft's angle of arrival (AOA).

References

1. B.R. Bean and E.J. Dutton, "Radio Meteorology," National Bureau of Standards, Monograph 92, U.S. Government Printing Office, Washington, D.C., March 1966.

2. Junho Choi, "Performance Comparison of Tropospherc Propagation Model: Ray Trac Analysis Results Using Worldwide Tropospheric Databases," Naval Research Laboratory, Washington, D.C., September 1997.

3 K. Takahashi, "Atmospheric Error in Range and Range Rate Measurements Between a Ground Station and Artificial Statellite," IEEE Trans. Aerosp. Electron. Syst. AES-6, 770-779 (1970).

4. G.H. Millman, "Atmospheric Effects on Radiowave Propagation," in Modern Radar: Analysis, Evaluation, and Design," R.S. Berkowitz, edited, John Wiley & Sons, Inc., New York, 1965.

5. H.S. Hopfield, "Two-quadratic Tropospheric Refractivity Profile for Correcting Satellite Data," J. Geophysics Research, (18), pp 4487-4499 (1969).

6. C.C. Goad and L. Goodman, " A Modified Hopfield Tropospheric Refraction Correction Model," Processings of American Geophysics Union, Fall Annual Meeting, San Francisco, California, December 1974.

7. T.D. Moyer, "Mathematical Formulation of the Double Precision Orbit Determination Program (DRODP)," Technical Report #32-1527, Jet Propulsion Laboratory, Pasadena, California, May 1971.

8. T.E. Gallini, "A Survey of Tropospheric Refraction Models," #TOR-94(4488)-11, The Aerospace Corporation, El Segundo, California, April 1994.

9. Louis J. Ippolito Jr., "Radiowave Propapagation in Satellite Communications," pubished by Van Nostrand Reinhold Company, New York, 1986.

10. K.C. Ho and Y.T. Chan, "Solution and Performance Analysis of Geolocation by TDOA," IEEE Trans. Aerosp. Electron Syst. AES-29, 1311-1322 (1993).

11. Foy, W. H., "Position-location solutions by Taylor series estimation," IEEE Trans. Aerosp. Electron Syst. AES-12, 187-194 (1976).

Appendix Eight Sites for Testing

	Site1	Site2	Site3	Site4	Site5	Site6	Site7	Site8
Latitude	22.4°	56.8°	51.9°	13.5°	-7.2°	38.8°	40.8°	47.8°
Longitude	292°	357.4°	183.4°	144.8°	72.3°	282.9°	141.3°	11.9°
Station Altitude (m)	2.912	65.13	82.43	152.29	20.50	29.11	32.83	495.95